

Journal of Materials Chemistry C

Accepted Manuscript



This is an *Accepted Manuscript*, which has been through the Royal Society of Chemistry peer review process and has been accepted for publication.

Accepted Manuscripts are published online shortly after acceptance, before technical editing, formatting and proof reading. Using this free service, authors can make their results available to the community, in citable form, before we publish the edited article. We will replace this *Accepted Manuscript* with the edited and formatted *Advance Article* as soon as it is available.

You can find more information about *Accepted Manuscripts* in the [Information for Authors](#).

Please note that technical editing may introduce minor changes to the text and/or graphics, which may alter content. The journal's standard [Terms & Conditions](#) and the [Ethical guidelines](#) still apply. In no event shall the Royal Society of Chemistry be held responsible for any errors or omissions in this *Accepted Manuscript* or any consequences arising from the use of any information it contains.

ARTICLE

Self-Assembly of One Dimensional DNA-templated Structures

Cite this: DOI: 10.1039/x0xx00000x

T. Catherall^a, D. Huskisson^a, S. McAdams^a and A. Vijayaraghavan^{a,b*}

Received 00th January 2012,

Accepted 00th January 2012

DOI: 10.1039/x0xx00000x

www.rsc.org/materials

Self-assembled DNA-templated structures have been an area of active development over recent years. They provide a cheaper, more practical bottom-up approach for producing nanostructures compared to current industry standards. This review focusses on recent developments in this field. Methods of synthesis are covered including the DNA templates used, how they are aligned, and self-assembly approaches taken. Characterisation is discussed including various imaging techniques and the electronic and optical properties that these structures possess. A broad range of applications are described including conductive nanowires, biosensors and thin film photonics.

1. Introduction

The concept of self-assembly represents an organic approach to bottom-up fabrication, and has seen rapidly increasing interest in recent years. This is clearly demonstrated by the rising quantity of papers published in the field, illustrated in figure 1. The topic was summarised by Whitesides and Gryzbowski in 2002,¹ coinciding with an acceleration in the rate of publication. An exact definition of self-assembly proves elusive, as many studies use the same catch-phrase for different processes. However, most now agree with the standard set by Whitesides that self-assembly chiefly consists of the spontaneous increase of order in a system without human intervention.

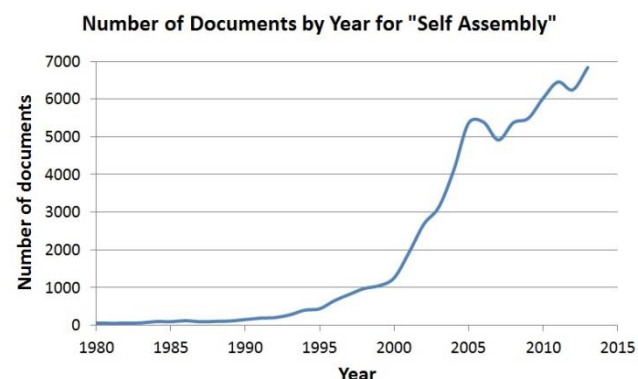


Figure 1: Number of documents published per year relating to "Self Assembly" from 1980 until 2013. Data taken from Scopus database.

There are many reasons why self-assembling systems are scientifically interesting and technologically important, as summarised by Whitesides and Boncheva.² Self-assembly is centrally important to life, as demonstrated by the living cell with its complex systems of lipid membranes, folded proteins, structured nucleic acids, protein aggregates and molecular machines.³ By understanding the processes involved, it will be possible to create more effective medicines, potentially reducing the need for invasive procedures. Self-assembly also creates materials with regular structures, such as molecular crystals, liquid crystals, semi-crystalline and phase separated polymers. Through self-assembly, small molecules can be used to build larger, complex systems with applications in materials and condensed matter science.⁴ Self-assembly provides a convenient strategy for creating complex nanostructures. Being a bottom-up technique, many materials can be produced quickly, easily and cheaply. Breakthroughs in self-assembled technology will also be easier to industrialise than their top-down alternatives as less investment will be required for manufacturing assets. As a result, self-assembly is and will continue to be important across a broad range of disciplines.

Self-assembled 1D structures are not reported as often as 2D thin films or 3D structures, yet they offer many unique and interesting properties and applications. The two main categories of interest are discrete arrays of 0D nanoparticles (NPs), often termed 'chains', and continuous structures, often termed 'nanowires'. 1D arrays of NPs promise novel photonic, electromagnetic and bio-sensing applications. A 2005 review describes novel waveguides, with unequal propagation of light in the parallel and perpendicular directions with respect to the chain.⁵ Anisotropy is also described for residual magnetisation

of chains when synthesised in magnetic fields of different orientations. Historically, research into continuous structures has largely focussed on electronic applications and the synthesis of conducting nanowires with novel electronic properties, such as high-temperature superconductivity.⁶ This trend has continued, with many studies investigating a wide range of materials for the assembly of nano-scale electronic components and circuitry.

DNA provides a mechanically robust scaffold for the directed self-assembly of 1D nanostructures. DNA is itself a well-defined self-assembling bi-polymer, with numerous attractive features for bottom-up nanoscale fabrication, such as (i) a diameter of 2nm yet a programmable length ranging from nanometres to microns; (ii) numerous bonding sites for matter in the form of aromatic bases and a polyanionic phosphate backbone; and (iii) the existence of well-established techniques for its synthesis, amplification and manipulation.^{7, 8}

DNA monomers are composed of a phosphate-deoxyribose sugar connected to one of four nucleotides: purines, adenine (A) and guanine (G); and pyrimidines, cytosine (C) and thymine (T). A chain of such monomers forms a single DNA strand, and providing that two single DNA strands have a complementary nucleotide sequence, i.e. C opposite a G, and an A opposite a T, a double-stranded DNA-helix will self-assemble as shown in figure 2.⁹

2. Synthesis of DNA-templated 1D Structures

This section will focus: (i) the DNA templates used, and if applicable, how they are synthesised and aligned on a substrate; and (ii) the approaches used to assemble a variety of materials into both continuous and discrete 1D structures.

2.1 DNA Templates. DNA templates are either: (i) non-periodic, i.e. genomic DNA with a 'random' nucleotide sequence; or (ii) periodic: synthesised to have a repeating nucleotide sequence.¹⁰ Commercially available genomic DNA is commonly used as a template without further modification as it is inexpensive and widely available.¹¹ The

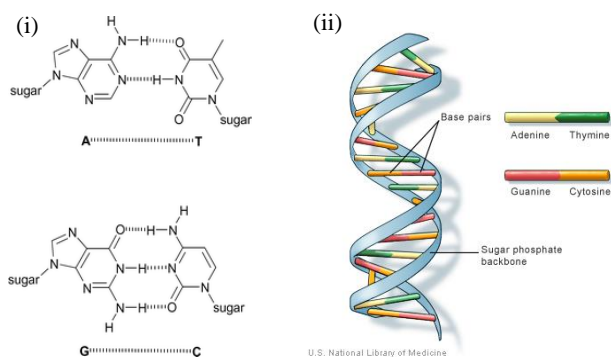


Figure 2: The DNA-double helix chemical composition and structure. (i) Complementary nucleotide bases: adenine (A) and thymine (T); and guanine (G) and cytosine (C).⁸ (ii) The double stranded DNA-helix.

most extensively employed template genome is the linear double stranded (ds) bacteriophage lambda-DNA (λ -DNA), which is approximately 48.5k nucleotides (16 μ m) in length.¹² *E. coli B* genomic DNA; calf-thymus DNA; and genomic DNA isolated from salmon have also been used.^{11, 13, 14} Additionally, the M13 bacteriophage genome is utilised in 'DNA origami' for assembling both continuous and discrete structures of complex geometries.¹⁵

Genomic DNA has been utilized in nanowire fabrication, wherein the polyanionic properties of DNA are exploited for the adsorption of cationic species; whilst the template nucleotide sequence itself is largely irrelevant. However, in numerous applications, DNA templates with a specific nucleotide sequence are desirable to allow for: (i) the spatially controlled templating of matter; or (ii) the creation of intricate DNA-template motifs.^{16, 17} For example, custom-made DNA strands have been utilised to synthesise complex self-assembled 'DNA tiles'.¹⁷ Whilst Coomber et al utilised a base-by-base oligonucleotide synthesiser to create a long DNA template from two staggered oligonucleotides containing 'A-T rich regions' for the attachment of Au NPs functionalised with DNA binding peptides.¹⁸ Although such solid-phase synthesis creates oligonucleotides of arbitrary sequences, errors are increasingly evident with sequences greater than 200 nucleotides. Although polymerase chain reaction (PCR) can produce longer DNA strands, this PCR product is limited by the available source DNA, such as genomic DNA that has no periodicity.^{10, 19} As such, a technique known as rolling circular amplification (RCA) has been utilised for the synthesis of long periodic single-stranded DNA (ssDNA)

2.1.1 Rolling Circular Amplification. For the self-assembly of linear NP chains, the use of a long repetitive DNA strand is ideal. During RCA, a DNA polymerase (commonly phage Φ 29 due to its excellent strand displacement properties) uses a short cyclic ssDNA (<100 nucleotides) to synthesise a long ssDNA (>10,000 nucleotides), which has a nucleotide periodicity complementary to that of the original strand, as shown in figure 3.^{20, 21} Deng et al. first utilised a 12 nucleotide-long ssDNA to synthesise a RCA strand up to 4 μ m in length for the directed self-assembly of phosphine-capped Au NPs.

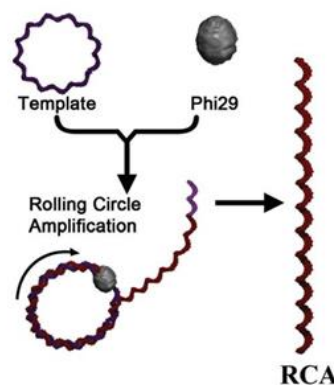


Figure 3: An illustration of the rolling circular amplification process. The bacterial polymerase Φ 29 utilises a short cyclic ssDNA to synthesise a long periodic ssDNA.²¹

Beyer et al utilised a 100 nucleotide template to synthesise a RCA strand up to 10,000 nucleotides in length.¹⁰ The periodic attachment of biotinylated ssDNA to the RCA strand directed the self-assembly of streptavidin-coated Au NPs. The RCA strand also contained a restriction site for the endonuclease ‘HNDIII’ that was utilised in further characterising the NP-DNA assembly. Similarly, Carneiro et al created a RCA strand of either 72 or 61 repeating nucleotides, depending on the original template used. The final RCA strands ranged from 1,400 to 15,000 nucleotides in length (0.5 to 5.1 μm), with a weighted average of 2,500 nucleotides. The RCA strands were used to synthesise DNA nanotubes that directed the self-assembly of co-block polymer/DNA hybrids.²¹ Recently an electrical sensor was fabricated using RCA to bridge a DNA template between two Au electrodes.²² Oligonucleotide-functionalised Au NPs bound to the DNA template, and a subsequent metallization step produced Au or Ag nanowires. Au nanowires were more homogenous, with a width of 300 nm. However, more complex DNA template designs may require a method known as ‘DNA origami’.

2.1.2 DNA Origami. In 2006, Rothemund pioneered a technique called ‘scaffolded DNA origami’, in which ssDNA from the M13 bacteriophage genome was folded into arbitrary 2D structures using complementary short synthetic oligonucleotides known as ‘staple strands’.²³ Whilst DNA origami has since been used to create complex 3D structures, 1D DNA origami geometries hold great promise for use in complex nanoelectronic circuits.^{15, 24}

Several papers have utilised this M13 scaffold to achieve desired geometries for templating.²⁴⁻²⁶ However, the use of full genomes, potentially thousands of nucleotides in length, as folding scaffolds limits the number of obtainable origami designs.¹⁹ This was overcome by Pearson et al who synthesised scaffold strands of different lengths (756 to 4808 nucleotides) using PCR on two genomic DNA templates: M13 and λ -DNA. Using biotinylated 3’ primers, one strand of the PCR product was isolated via binding to a streptavidin-coated magnetic bead, and subsequent DNA denaturation. The non-biotinylated ssDNA was then combined with staple strands to yield DNA origami of a programmed conformation.¹⁹ This method has since been used by Pearson et al for the synthesis of a range of DNA origami geometries, used for directing both discrete and continuous 1D structure self-assembly.¹⁵

2.2 DNA Template Supramolecular Organisation

2.2.1 DNA Origami. A range of DNA origami templates have been utilised in the directed self-assembly of 1D structures as shown in figure 4. For example, Pearson et al. demonstrated the formation of a ‘T’ shaped template, in addition to a circular circuit origami structure.¹⁵ The latter structure was similarly developed by Geng et al.²⁶ Geng et al²⁴ previously reported an elongated DNA nanowire structure using λ -DNA, and a branched DNA origami scaffold. Bui et al folded a M13 scaffold into six-helix nanotube bundles, 412 nm in length and 6 nm in diameter.²⁵ Similarly, a 24-helix bundle was created by Kuzyk et al.²⁷

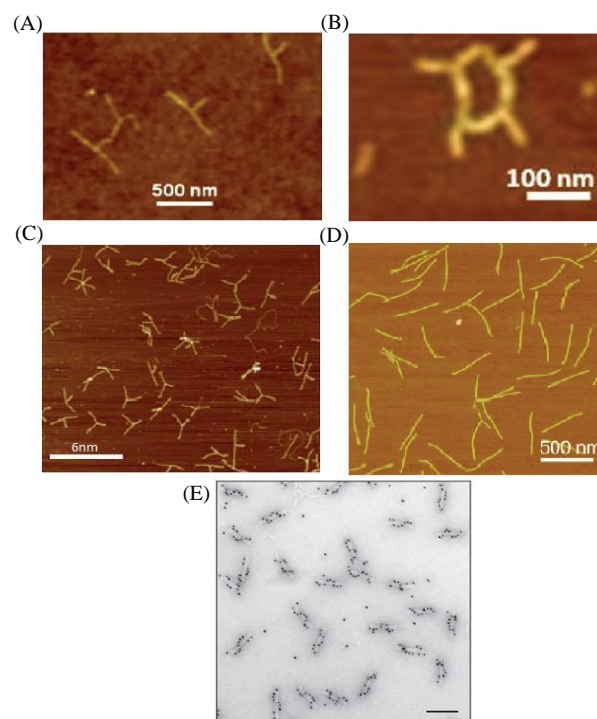


Figure 4: DNA origami template examples. (A) Atomic Force Microscopy (AFM) image of T-shaped origami structures. (B) AFM image of a circular circuit origami structure. Reprinted with permission from *J. Phys. Chem. B*, 2012, **116**, 10551. Copyright 2012 American Chemical Society. (C) Branched DNA origami structures.²⁴ (D) AFM image of six-helix nanotube origami bundles. Reprinted with permission from *Nano Lett.*, 2010, **10**, 3367. Copyright 2010 American Chemical Society. (E) Transmission Electron Microscopy (TEM) image of left-handed 24-helix origami bundles with Au NPs attached (scale bar = 100 nm). Reprinted by permission from Macmillan Publishers Ltd: *Nature*, 2012, **483**, 311. Copyright 2012.

2.2.2 Unique DNA Template Motifs. Several stand-alone higher order DNA template structures have been created without the use of DNA origami. Yan et al produced a four armed DNA tile, consisting of nine oligonucleotides that self-assembled to form long 1D nanoribbons, as shown in figure 5.

Park et al created a 1D three helix bundle consisting of nine oligonucleotides, which formed three double helical DNA domains connected via six immobile cross-over junctions. Using this template, Ag nanowires were assembled via electroless deposition to yield nanowires 30 nm in width and 2 μm in length, as shown in figure 6.¹⁶ DNA template supramolecular organisation can be determined by other factors. Pruneanu et al created polypyrrole nanowires using a pyrrole polymerisation solution in the presence of a λ -DNA template. However, whilst a reaction time of 3 hours resulted in thin nanowires 1 - 3 nm in diameter; an incubation time of 1 - 6 days resulted in the polymer-DNA strands braiding to irreversibly form ‘nanoropes’ 5 - 30 nm in diameter, possibly due to the shielding of DNA phosphate anions by multivalent cations. The

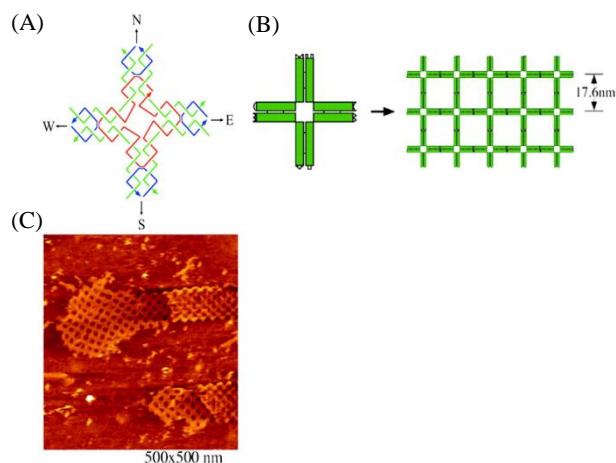


Figure 5: Self-assembly of DNA tiles to form nanoribbons. (A) The 4x4 tile consists of nine oligonucleotides, with each arm orientated in one of four directions: N, S, E, W. (B) (i) Complementary tile ends are depicted as tessellating geometric shapes, which self-assemble into a DNA tile lattice. (C) AFM image (500nm x 500 nm) of a 1D nanoribbon. From *Science*, 2003, **301**, 1882. Reprinted with permission from AAAS.

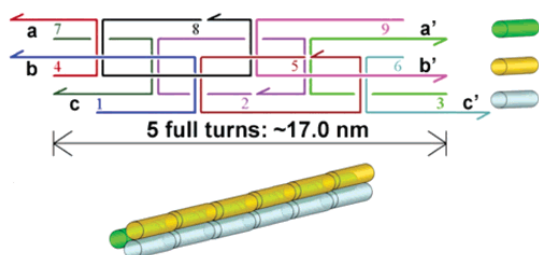


Figure 6: Three helix bundle DNA tiles. The structure consists of nine oligonucleotides that form three duplexes (paired horizontal lines and cylinders) with six crossover junctions (paired vertical lines). Coloured arrows of oligonucleotides represent strands in a 5' to 3' direction. Complementary sticky-ends of a, b, and c are a', b', and c' respectively. Reprinted with permission from *Nano Lett.*, 2005, **5**, 693. Copyright 2005 American Chemical Society.

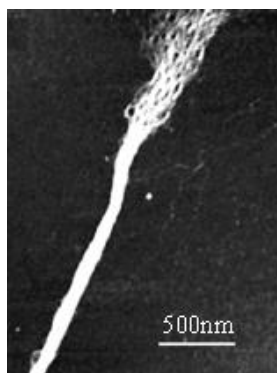


Figure 7: Polypyrrole nanoropes. AFM image of λ -DNA-templated polypyrrole nanoropes. Note the 'frayed ends', which confirms the rope-like structure. From *Adv. Funct. Mater.*, 2008, **18**, 2444. Reproduced with permission from John Wiley and Sons.

structures were subsequently deposited and aligned on a silicon substrate for further characterisation as shown in figure 7.⁷

2.3 DNA Template Alignment.

Due to thermal fluctuations, DNA in solution has the propensity to coil, and form random structures.²⁸ The application of DNA-templated 1D nanostructures in devices will likely necessitate control over template directionality once deposited on a substrate. Whilst a low-cost and scalable DNA nanowire aligning technique remains elusive, various techniques are available, and are covered by Gu et al.^{28, 29} This section will focus on techniques used to align DNA templates specifically used to direct the self-assembly of 1D structures.

DNA templates can be aligned (or 'combed') on substrates via bulk fluid flow, or a moving air-liquid interface.³⁰ The former relies on a DNA solution being propelled in a single direction along a substrate surface; the consequential fluidic flow aligns the sporadically adhered DNA molecules in parallel along the direction of flow.⁷ For example, Deng & Mao combed λ -DNA prior to the plating of Pd to form highly aligned nanowires. Briefly, a DNA/ Mg^{2+} solution was deposited on a glass slide or mica substrate. Compressed air propelled the solution directionally along the substrate, stretching DNA templates into parallel chains in centimetre long trenches. The authors note that the quality of DNA alignment is dependent upon two factors: (i) Mg^{2+} concentration: Mg^{2+} mediates the attachment of the polyanionic DNA to the negatively charged mica substrate. Whilst at low Mg^{2+} concentrations (<0.05 mM) DNA will not attach to the substrate, at high concentrations (>1 mM), DNA will form arbitrary networks and coils; and (ii) flowing velocity: through differing propulsion speeds, the extent of DNA straightness and density could be controlled, as shown in figure 8.¹² 0.5–2 cm/s was identified as an optimal speed in previous work.³¹ Furthermore, additional factors in determining DNA alignment quality using this technique have been identified: (i) the angle of the applied compressed air relative to the substrate; (ii) DNA concentration; and (iii) incubation time.³¹ Additionally, substrates can also be modified with a self-assembled monolayer to enhance hydrophobicity, which augments adsorption of the DNA hydrophobic core to the substrate.^{32, 33}

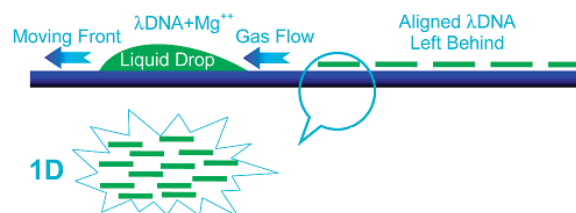


Figure 8: Molecular combing of λ -DNA onto a mica or glass substrate. Compressed air drives the DNA/ Mg^{2+} solution directionally along the substrate, producing aligned λ -DNA. Reprinted with permission from *Nano Lett.*, 2003, **3**, 1545. Copyright 2003 American Chemical Society.

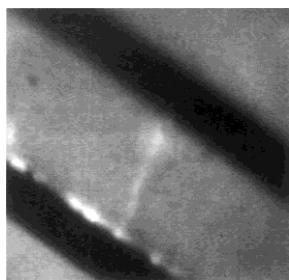


Figure 9: A DNA bridge. Fluorescently labelled (YOYO-1) λ -DNA stretched 16 μ m between two Au electrodes (black lines). Reprinted with permission from Macmillan Publishers Ltd: *Nature*, 1998, **391**, 775. Copyright 2012.

The driving force for the DNA solution across a substrate can take additional forms, such as the use of pipette tips; kimwipe papers; or a XYZ translation stage.^{7, 34, 35} Pruneanu et al utilised a pipette tip to drag a DNA solution between two Au microelectrodes in order to measure electrical conduction properties of DNA-templated polypyrrole nanowires.⁷ Similarly, Braun et al induced a fluidic flow to attach a DNA template between two Au electrodes (a DNA ‘bridge’) functionalised with short complementary oligonucleotides as shown in figure 9.³⁶

Additionally, the use of a moving air-liquid interface in the form of a receding meniscus, allows DNA to be combed along a substrate to achieve a uniform directionality.³⁷ During this, DNA solution is deposited on a substrate, and strands sporadically adsorb to the substrate surface. Capillary forces found at the receding front of the

evaporating solution will align the DNA strands along the substrate surface perpendicularly to the meniscus front.³⁸ Recently Li et al aligned a λ -DNA solution by means of a receding meniscus using either a spherical or cylindrical lens atop a flat substrate, where pH and temperature were important determinants of alignment quality. Whilst this is claimed to be a low cost and simple technique for DNA-based nanostructures, the alignment of such structures using this technique has yet to be demonstrated.²⁹

Other variations of such molecular combing techniques have been utilised in templating 1D structures. For example, during spin-stretching, rotational flow is induced via a viscous force that aligns DNA strands along a substrate.³⁹ Lastly, low energy ion irradiation was used to pattern nanoscale ripples onto a substrate with periodicities between 20 nm and 50 nm.⁴⁰ Charged oxides on the substrate surface subsequently directed DNA origami tubes to the base of the ‘ripple valleys’ where a parallel alignment was observed.

2.4. Self-assembly Approaches.

DNA-templated matter can be broadly categorised into discrete or continuous structures. The former describes templated matter separated by a periodic ‘gap’ region. Such synthesis provides a facile method to generate programmable and tunable linear NP arrays.¹¹ The latter describes an unbroken length of matter, which bestows attractive properties to templated structures, most notably electrical conduction in DNA-templated nanowires. Here, the various techniques used in the assembly of such structures are detailed, as summarised in table 1.

Table 1: Summary of various types of structures synthesised using a range of self-assembly DNA-templating techniques.

Continuous Metallic			
Structure	Synthesis	DNA	Reference(s)
Ag nanowire	Development of reduced Ag ⁺ acidic solution.	λ -DNA	35
Pd nanowire	Activation, reduction and electroless plating.	λ -DNA	12, 32, 37, 40
Pd nanowires and Au nanostructures.	Pd or Au plating on Pd-seeded DNA.	λ -DNA or DNA origami	23
Au nanostructure	Attachment of DNA-modified Au NPs to staple strands, followed by metallisation.	DNA origami	15
	Electroless metallisation of +ve Au NPs seeds.	DNA oragami	43
Cu nanowires	Reduction of Pd ²⁺ seeds – Cu electroless plating.	λ -DNA	44
	Activation, reduction and electroless plating.	λ -DNA	34
Cu ₂ O nanowires	Activation, reduction and electroless plating.	λ -DNA	46
Magnetic nanowire	Electrostatic interactions.	λ -DNA	47, 48
Co nanowires	Pd ²⁺ seed reduction then Co electroless plating.	λ -DNA	49
Magnetite	Fe ²⁺ and Fe ³⁺ activation then coprecipitation of Fe ₃ O ₄ , with increasing the solution pH.	λ -DNA	50
Au nanowires	Photo-induced reduction of Au ions.	DsDNA isolated from salmon testes	14

Discrete Metallic

Structure	Synthesis	DNA	Reference(s)
Au NP Array	DNA-modified Au NPs	RCA Template	20
	Oligonucleotide modified Au NPs	DNA Origami	26
	Au NPs coated with DNA-binding Peptide	Synthetic DNA	18
	Streptavidin-coated Au NPs bound to periodically biotinylated DNA	RCA strand	10
	Streptavidin-coated Au NPs	DNA Tiles	17
	Cationic headgroup in the ligand shell of Au NPs,	λ -DNA	51

Continuous Polymeric

Structure	Synthesis	DNA	Reference(s)
Polymer nanowire	Oxidation of monomers.	λ -DNA or calf thymus DNA	52, 53, 54, 56, 57, 58

Discrete polymeric

Structure	Synthesis	DNA	Reference(s)
DNA nanotubes	PEG-DNA conjugates.	RCA strand	21
Polyaniline nanowires	Ru(bpy) ³²⁺ -catalyzed photopolymerization of polyaniline between cationic Au NPs.	λ -DNA	59

Continuous Semiconductor

Structure	Synthesis	DNA	Reference(s)
CdS nanowires	Cd(NO ₃) ₂ with Na ₂ S.	λ -DNA	60
Te and Bi ₂ Te ₃ nanowires	Ag seeds a template for the electroless deposition of Ni and Cu converted to Te or Bi ₂ Te ₃ by a galvanic displacement reaction.	λ -DNA	63
CuS nanowires	CuCl ₂ reacted with either Na ₂ S or HS.	λ -DNA	39
BaWO ₄ nanowires	Ba(NO ₃) ₂ with Na ₂ WO ₄ .	<i>E. coli</i> genomic DNA	11
CdS nanowires	Incubated cadmium perchlorate, and C ₂ H ₅ NS in presence of microwave radiation.	λ -DNA	63

Discrete Semiconductor

Structure	Synthesis	DNA	Reference(s)
QD Array	Streptavidin-conjugated QDs with staple strands modified with biotin.	DNA Origami	24
CdS array	Positively charged CdS NPs.	SsDNA isolated from salmon testes	64
CdSe/ZnS QDs arrays	Electrostatic interactions.	λ -DNA	65, 66

2.4.1 Continuous Metallic Structures. With the exception of short strands, DNA alone is a poor conductor, and hence has limited use in electronic applications.⁴¹ However, DNA metallization offers means by which the electrostatic properties of DNA can be exploited to produce continuous and conductive metallic nanowires. DNA metallization commonly consists of three main steps: (i) the activation step, in which metal cations adsorb to the polyanionic DNA backbone, or are introduced between nucleotide bases; (ii) the reduction step, in which a reducing agent transforms the ions into fixed metal zero-valence nanoclusters; and (iii) the growth step, in which the metal nanoclusters act as both a nucleation site and catalytic surface for the further reduction of metal ions, and consequential growth of metallic structures.³³

This process was first introduced by Braun et al through templating 12 μm long and 100 nm wide conductive Ag nanowires on λ -DNA between two Au electrodes.³⁶ However, this process required an additional ‘development’ step using an acidic solution of hydroquinone and Ag ions to form a continuous structure. Richter et al subsequently templated Pd nanowires on λ -DNA without such a development step.⁴² This was first accomplished in solution, in which DNA was activated using Pd^{2+} ions for two hours; followed by a chemical reduction of the adsorbed metal ions by dimethylamine borane (DMAB) to produce Pd clusters 3 - 5 nm in diameter within seconds. With a prolonged reduction step of 1 minute, a quasi-continuous coverage was ascertained, with a Pd cluster size of 20 nm in diameter. This ultimately resulted in 5 μm long quasi-continuous nanowires 20 - 40 nm in width. The process was repeated by aligning λ -DNA on a glass slide substrate prior to the reduction step, which again formed Pd clusters along the DNA template. This was important as DNA alignment on a substrate post-metallisation is not possible as the molecular recognition properties of DNA are consequently destroyed.³³ Richter et al later reintroduced multiple developing steps by sequentially adding the Pd solution and reducing agent multiple times: enabling the controlled growth of both discrete and continuous Pd structures, as shown in figure 10.³⁸ Deng & Mao similarly reduced Pd^{2+} ions adsorbed to aligned λ -DNA using DMAB.¹² Importantly, it was found that both shortened activation and reduction steps produced more uniform nanowires less than 30 nm in width that were free of random branches.

Nguyen et al established a technique that addressed the rapid reaction rate of the DMAB reducing agent with Pd^{2+} ions to allow for increased control over the growth step, consequently producing a

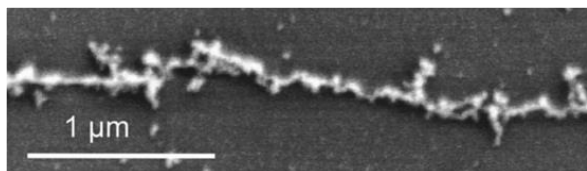


Figure 10: A λ -DNA-templated Pd nanowire. SEM image of a Pd nanowire greater than 40 nm in width after one development step (see text). Branching structures result from stochastically determined metallisation of the template. Reprinted with permission from *Appl. Phys. Lett.*, 2001, **78**, 536. Copyright 2001, AIP Publishing LLC.

more uniform Pd metallisation.³³ Initially, the λ -DNA template is combed onto a hydrophobic-coated substrate to reduce nonspecific metallization. The DNA is then incubated with palladium chloride, which is hydrolysed to form PdO. The polar PdO selectively binds to the polyanionic DNA backbone at a slow, and hence controllable rate. The reduction of PdO to metallic Pd subsequently forms highly uniform nanowires with a minimum width of 20 nm, and a maximum continuity of 3 μm when grown optimally for 42 hours at 45°C. Interestingly, if the reduction step was accomplished using hydrogen gas, a more ‘robust’ Pd nanowire was formed, with a resistance 3 orders of magnitude lower than DMAB reduced nanowires. However, the slow metallization step of 2 days is unattractive in terms of scalability.

As such, Geng et al established a quicker Pd metallisation process, investigating the minimum activation time required to give a high Pd seeding density; initially on a λ -DNA template.²⁴ Whilst seeding densities increased with activation times up to 30 minutes, it did not significantly increase above 10 minutes. Consequently, the authors used this optimised seeding method to plate DNA origami structures with Pd and Au with good selectivity to achieve nanowires ~30 nm in width. It was found that seeding density was relatively higher on DNA origami templates (1 seed per 70 nm) compared to λ -DNA (1 seed per 115 nm). This was an improvement over the authors’ previous efforts to metallise DNA origami, which resulted in low seeding densities using a relatively convoluted metallisation process.⁴³

Pearson et al further improved the metallization of DNA origami in several respects: achieving a higher seeding density at specific sites along the DNA origami template.¹⁵ Previous work on site-specific metallisation used aldehyde derivatization of DNA as a localised reducing agent of Ag ions.⁴⁴ However, site-specific metallisation of DNA origami to produce controlled gap regions could provide the means to fabricate more intricate nanocircuitry. The group used a standard M13 scaffold, which was folded into a branched ‘T’ shape using staple strands as previously described. Importantly however, the staple strands in select locations along the top of the ‘T’ were

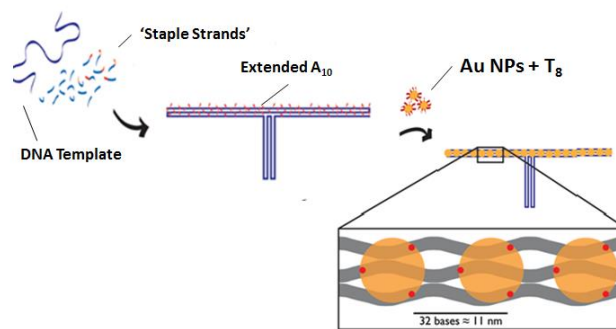


Figure 11: Site-specific seeding of DNA origami with functionalised Au NPs. Staple strands (blue) modified with an extended adenosine chain (A_{10}) fold the DNA template into a T-shaped structure. Au NPs coated with oligonucleotides (T_8) complementary to the modified staples selectively seed along the top of the structure. Adapted with permission from *J. Phys. Chem. B*, 2012, **116**, 10551. Copyright 2012 American Chemical Society.

extended with an adenosine chain. Au NPs (5 nm in diameter) conjugated to a thiolated thymine chain were combined with the DNA template either in solution or on a silica substrate to form Au seeds at these specific sites. The seeded structure was ~240 nm in length and contained 67 staple strands which bound ~22 Au NPs at a 1:3 ratio, as shown in figure 11.

The Au seeds were subsequently plated with further Au to form continuous structures. The quality and width of the continuous structure was proportional to the length of the plating step. For example, whilst the plating width of Au seeds after 1 minute was insufficient to bridge larger gaps between seeds (>12 nm), a plating step of 2 minutes resulted in continuous Au coverage, as shown in figure 12. Similarly, a plating step of 5 minutes or 20 minutes resulted in nanowire widths of 18.3 ± 6.1 nm; and 25 ± 11.4 nm respectively. Nanowire widths at longer plating times showed increased variability in width, demonstrating a ‘beads on a string’ morphology, as shown in figure 12C. The authors also showed the selective plating of a circular circuit DNA origami template to form a rudimentary logic gate structure. Recently, the Pd seeding uniformity and density of this origami structure was increased using multiple (up to five) plating steps.²⁶

Additional examples exist of DNA origami metallization: 1.4 nm Au NPs coated with positively charged amines were seeded onto 428 nm long six-helix bundles in either solution, a carbon-coated grid or silicon wafer. To prevent aggregation of components in the seeding solution, the concentration of Au NPs was vastly higher than the DNA. After metallisation, the mean nanowire length was 438 ± 70 nm, with a width of $56 \text{ nm} \pm 8$ nm.⁴⁵

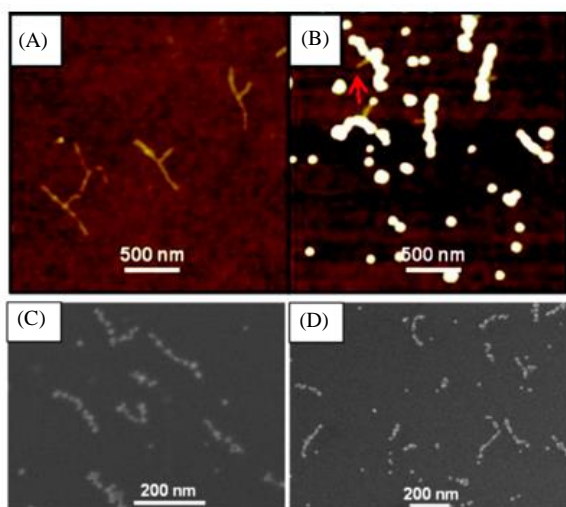


Figure 12: Au plating of Au NP seeds on T-shaped DNA origami. (A) AFM image of unseeded DNA origami structures. (B) AFM image of Au plated DNA origami structures. The red arrow points to the unseeded portion on the origami. (C) Scanning Electron Microscopy (SEM) images of plated DNA origami structures after (i) 1 minute; and (ii) 2 minutes. Note the ‘beads on a string’ morphology after 1 minute of plating. Adapted with permission from *J. Phys. Chem. B*, 2012, **116**, 10551. Copyright 2012 American Chemical Society.

Cu is commonly used as interconnects in integrated circuits. The generation of Cu nanowires using bottom-up approaches, such as DNA templating, offers a potentially cheaper and more practical option to current industry standards.⁴⁶ Kudo et al first templated Cu nanowires: λ -DNA was seeded with Pd^{2+} ions, and subsequently reduced to Pd0, forming Pd nanowires ~6 nm in width.⁴⁷ The metallic Pd then acted as seeds for the electroless deposition of metallic Cu, through the reduction of Cu^{2+} with formaldehyde. It was found that Cu nanowire width correlated with plating time. Subsequently, Monson and Wooley described a process for the generation of Cu nanowires templated on Si-immobilised λ -DNA using the seeding/reduction methodology previously described.³⁵ Briefly, λ -DNA was incubated with an aqueous solution of $\text{Cu}(\text{NO}_3)_2$; and the Cu^{2+} ions interacted with the polyanionic DNA backbone. The reduction of the Cu^{2+} ions by ascorbic acid formed a metallic copper sheath ~3 nm in height around the template DNA. However, due to the large horizontal dimensions of the Atomic Force Microscope (AFM) tip, establishing whether continuous or discrete structures were formed was not possible. Watson et al used a similar protocol but on substrate aligned λ -DNA.⁴⁶ The templated structures had a ‘beads-on-a-string’ morphology, and a consequential high electrical resistance. Hassanien et al recently demonstrated through the use of an alkaline cupric citrate solution (Benedict’s reagent), and ascorbic acid as a reducing agent, cuprous oxide templated onto λ -DNA in solution to form conductive nanowires 12–23 nm in diameter along the length of the DNA template.⁴⁸

Magnetic NPs have a plethora of potential applications, most notably with regards to storage media. A common technique for self-assembly of magnetic NPs exploits the electrostatic interaction between cationic NPs and polyanionic DNA. For example, dense magnetic NP arrays were generated in solution using Fe_3O_4 NPs with a positively charged shell that self-assemble onto polyanionic λ -DNA.⁴⁹ Using a similar protocol, Fe_3O_3 NP structures in solution have also been formed.⁵⁰

Other techniques exist for the creation of DNA-templated magnetic nanowires. Gu and Hynie describe a two-step process for the generation of Co nanowires.⁵¹ Initially, Pd NP clusters are generated on a λ -DNA template following the standard activation/reduction methodology described previously. The seeded Pd NPs are essential for the reduction of Co ions to form Co nanowires 40 – 60 nm in width, in both solution and on a silicon substrate. Recently, magnetite (Fe_3O_4) phase iron oxide nanowires were formed through the association of Fe^{2+} and Fe^{3+} to λ -DNA, which were transformed to Fe_3O_4 via an increased pH brought about through the addition of NaOH.⁵² Watson et al demonstrated a novel method for the preparation of DNA-templated magnetic nanowires through electrochemical reduction.³² Essentially, an aqueous solution of λ -DNA and Fe^{2+} was dropped onto an n-doped Si wafer, where the cations adsorbed to the polyanionic DNA template. The wafer acted as an electrode for the electrochemical reduction of the DNA bound Fe^{2+} to Fe. This Fe acted as a nucleation site for further Fe deposition and growth over the DNA template to form dense linear NP arrays 2 - 26 nm in diameter.

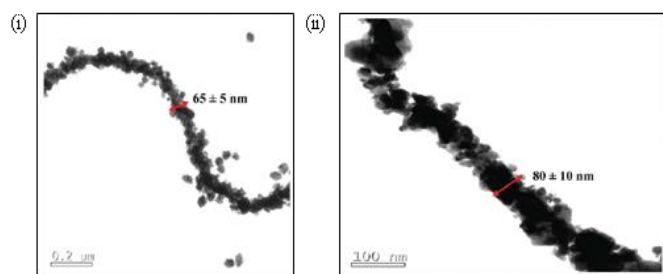


Figure 13: Self-assembly of Au nanowires via the UV reduction of Au(III). TEM images of Au nanowires at different DNA: Au (III) salt ratios: (i) 1.2M : 2.43M ; and (ii) 1.18M : 3.38M.¹⁴

Lastly, metallic nanowire structures were generated using a photo-induced reduction of Au ions. An Au(III) salt solution was mixed with dsDNA (isolated from salmon testes), and subsequently exposed to UV irradiation for ~4 hours, reducing Au(III) to Au⁰. Consequently, Au NPs 12 – 45 nm in diameter adsorbed densely to the DNA template over microns to form nanowires 12 – 80 nm in width, depending on the DNA to Au(III) ion ratios used, as shown in figure 13.¹⁴

2.4.2 Discrete Metallic Structures. Deng et al created linear NP assemblies using phosphine-capped NPs (5 nm in diameter) functionalised with 53 base pair (bp) DNA fragments complementary to a RCA strand. Up to 4 μm long 1D arrays of Au NPs, consisting of both entangled and wire like segments, were formed with a mean inter-particle spacing of 18.5 ± 6.9 nm, as shown in figure 14.²⁰

Furthermore, Kuzyk et al recently used DNA origami to create both left and right-handed 24 helix bundles, approximately 16 nm in diameter, with nine attachment sites for Au NPs (10 nm in diameter).²⁷ The attachment sites were three 15 nucleotide long extended staple strands that were complementary to the multiple thiol-modified oligonucleotides carried on the Au NPs. NPs and templates were mixed for 24 hours, purified using agarose gel electrophoresis, and imaged under TEM: a 98% success rate was found for the attachment of NPs to the template, with an average interparticle spacing of 11.22 ± 1.4 nm. However, structures with unbound NP sites after three months storage at 4 °C had a propensity to aggregate. Additionally, the helix monomers could be polymerised using a ‘polymerization oligonucleotide’ that was added to the left-handed nanohelix monomer solution, and allowed to polymerise for 12 hours, as shown in figure 15.

Self-assembled oligonucleotide templates have been used to organise NPs functionalised with DNA binding peptides. Au NPs were coated with two different peptides: (i) CALNN, which promotes cell



Figure 14: TEM image of Au NPs templated on a RCA strand (scale bar = 200 nm). From Z. Deng, Y. Tian, S. H. Lee, A. E. Ribbe and C. Mao, *Angew. Chem. Int. Ed.*, 2005, **44**, 3582. Reproduced with permission from John Wiley and Sons.

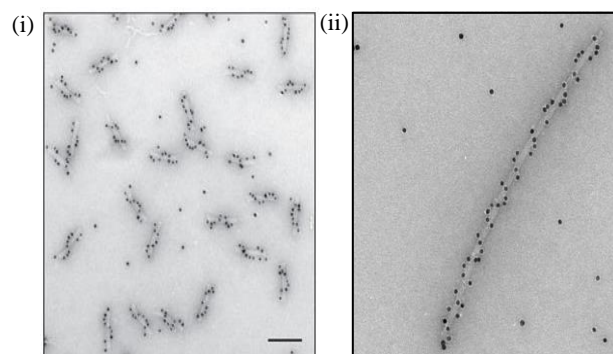


Figure 15: Left-handed Au NP helices. TEM images of: (i) left-handed helix monomers; and (ii) a left-handed nanohelix polymer constructed using six monomers (scale bar = 100nm). Reprinted with permission from Macmillan Publishers Ltd: *Nature*, 2012, **483**, 311. Copyright 2012

internalisation of NPs; and (ii) FQGII, which binds selectively to ‘A-T-rich regions’ of short DNA duplexes with high affinity.

Two templates were synthesised: a long template constructed from two staggered oligonucleotides, which generated long chains of NPs; and a short self-complementary sequence, which bound around the Au NPs, as shown in figure 16.¹⁸ It was found that through varying the surface concentration of FQGII, the authors could form 1D arrays of dimers, trimers, and using template 1, NP chains up to 3 μm in length. This was attributed to an alteration in the number of DNA binding events and rate.

NP self-assembly is also possible via the binding of streptavidin-coated Au NPs to a periodically biotinylated DNA strand. Beyer et al augmented a RCA template with complementary biotinylated DNA strands to form a DNA duplex.¹⁰ 5 nm streptavidin-coated Au NPs were added to the template to form 1D Au NP chains, as shown in figure 17. The chains had an inter-particle spacing of ~30 or ~50 nm, meaning that NPs bound to every available binding site, with an

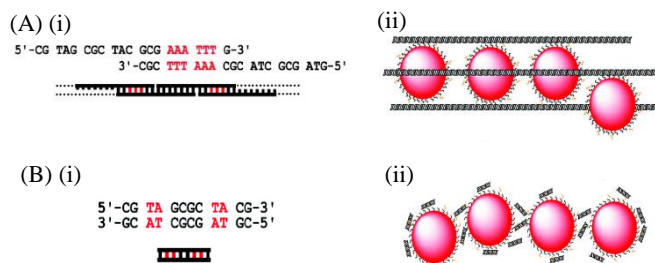


Figure 16: DNA Templates used for the directed self-assembly of Au NPs functionalised with DNA binding peptides (A) (i) The sequence of two staggered oligonucleotides that form a long DNA template for the creation of (ii) long chains of Au NPs. (B) (i) The sequence of the short self-complementary sequences that (ii) binds around Au NPs, giving limited control over NP organisation. Red nucleotides represent potential binding sites for DNA binding peptides. Adapted with permission from D. Coomber, D. Bartczak, S. R. Gerrard, S. Tyas, A. G. Kanaras and E. Stulz, *Langmuir*, 2010, **26**, 13760. Copyright 2010 American Chemical Society.

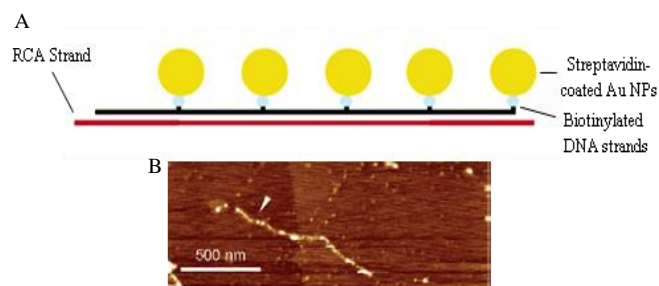


Figure 17: Streptavidin-coated Au NPs self-assembled using a RCA strand. (A) Illustration of the self-assembled structure: the RCA product was hybridized to biotinylated ssDNA, and subsequently incubated with streptavidin-coated Au NPs. (B) AFM image of a dense Au NP chain. Adapted with permission from *Nano Lett.*, 2005, 5, 719). Copyright 2005 American Chemical Society.

occasional gap of a single unoccupied biotin. The templated lengths depended upon the RCA template size, which can range from hundreds of nanometres, to a few micrometres.

Similarly Cheng et al utilised streptavidin-coated Au NPs in combination with a 4x4 DNA tile.¹⁷ The tile consisted of nine oligonucleotides, one of which was augmented with a biotin attachment. The DNA tiles had modified sticky ends enabling the assembly of a 1D ribbon-like template. Under TEM, NP interspacing distance was 15.8 - 19.4 nm, which was consistent with theoretical values. However, not all binding sites were utilised due to an 'imperfect binding efficiency'.

Additional DNA templating methodologies include exploiting the electrostatic interactions between a cationic headgroup in the ligand shell of Au NPs, with the polyanionic λ -DNA backbone. Warner and Hutchinson used this process to create linear Au NP assemblies up to 1 μm in length; with an inter-particle spacing of 1.5 nm due to neighbouring ligand shells. To reduce non-specific binding of the NPs to a substrate, the discrete structures were generated in solution.⁵³

2.4.3 Continuous Polymeric Structures. Polymer nanowires concomitantly hold the attractive electrical and optical properties of semiconductor metals, and the durability and compatibility of organic materials.⁵⁴ Synthesis of polymer nanowires involves the chemical oxidation of cationic monomers electrostatically bound along a polyanionic DNA template. Dong et al generated 'beads-on-a-string' polypyrrole nanowires on λ -DNA immobilised on mica using an FeCl_3 oxidant; whilst in solution, more uniform widths were observed.⁵⁵ The authors suggest that template immobilization on a substrate interferes with polymer growth. Contrastingly, Ma et al synthesised uniform polyaniline nanowires enzymatically via the addition of horseradish peroxidase (HRP) and H_2O_2 successively on λ -DNA immobilised on a silicon substrate.⁵⁶ The authors did not observe the agglomeration of DNA-templated polyaniline nanowires on the substrate, as was previously presented by Nagarajan et al due to the blocking of charged phosphate groups by the partially charged

polyaniline.⁵⁷ Moon et al polymerized polypyrrole nanowires using ammonium persulfate as an oxidant on DNA immobilised on a silicon wafer to form highly uniform nanowires.⁵⁸ Nickels et al used a similar polymerisation step but in solution, and found continuous structures forming.⁵⁹ Hassanien et al synthesised in solution uniform 5 - 30 nm polyindole nanowires on a λ -DNA template using an FeCl_3 oxidant.¹¹ Recently, 2,5-(bis-2-thienyl)-pyrrole (polyTPT) nanowires were polymerised in solution using a FeCl_3 oxidant on either λ -DNA or calf-thymus DNA, depending on the characterisation techniques employed.⁵⁴ Despite the TPT monomer lacking several hydrogen bonding sites as compared to pyrrole (which are important for monomer-DNA association), AFM images reveal uniform continuous nanowires 7 - 8 nm in width.

2.4.4 Discrete Polymeric Structures. Examples of discrete DNA-templated polymer structures are limited. Carneiro et al used a RCA template to construct DNA nanotubes onto which polyethylene glycol (PEG)-DNA conjugates were positioned via complementary base pairing, as shown in figure 18.²¹

Recently, an Au NP-polyaniline hybrid nanowire was created: cationic Au NPs (1.5 nm in diameter) were adsorbed onto a λ -DNA template, forming a discrete NP array. Subsequently, a $\text{Ru}(\text{bpy})_3^{3+}$ -catalysed photopolymerization of polyaniline generated polyaniline sections between the Au NPs, hence forming a pseudo-continuous structure.⁶⁰

2.4.5 Continuous Semiconductor Structures. Semiconductor NPs hold unique optoelectronic properties due to quantum confinement effects. Synthesis of DNA-templated semiconductor NPs traditionally involves two main steps: (i) the adsorption of metal ions to template DNA over an extended period of time (hours to days); and (ii) the reaction of the metal ion-DNA complex with a

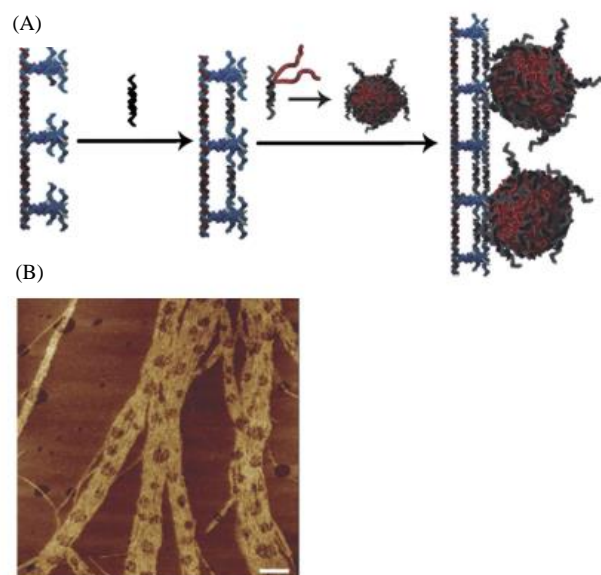


Figure 18: (A) Illustration of PEG-DNA conjugates positioned along RCA nanotubes. (B) AFM image of PEG-DNA conjugates along the RCA nanotubes (scale bar = 1 μm).²¹

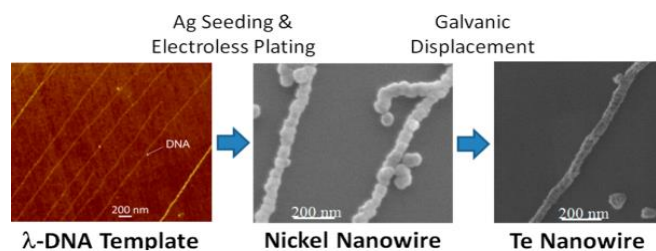


Figure 19: λ -DNA-templated Te nanowires by galvanic displacement. Reprinted with permission from *Langmuir*, 2013, **29**, 11176. Copyright 2013 American Chemical Society.

chalcogenide compound to produce semiconductor NPs.^{61, 34} The synthesis of discrete structures was first demonstrated by Coffey et al in solution using calf-thymus DNA incubated with a Cd^{2+} solution, and subsequently S^{2-} , to form CdS clustered NPs.⁶¹ The group reported a similar study in which immobilised circular plasmid DNA on a poly-lysine glass slide templated an array of CdS NP clusters formed from a reaction of Cd^{2+} and H_2S .⁶²

Dong et al reacted $\text{Cd}(\text{NO}_3)_2$ with Na_2S to template λ -DNA with CdS in both solution and on a silica or mica substrate.⁶³ Whilst a 'beads-on-a-string' morphology was achieved on substrate immobilised λ -DNA, a more continuous and uniform structure was produced in solution. Furthermore, NP coverage could be increased if the reaction mix was left to stand for a number of days, which also resulted in a small reduction in nanowire width (14 ± 1 nm to 12 ± 0.67 nm). However, Liu et al highlight that this technique is: (i) time-consuming; (ii) results in non-specific NP deposition; (iii) is restricted to particular materials; and (iv) lacks control over nanowire dimensions.³⁴ As such, the group provide a novel method to synthesis DNA-templated Te and Bi_2Te_3 nanowires: Ag-seeded λ -DNA aligned on a hydrophobic surface served as a template for the electroless deposition of Ni and Cu to form continuous nanowires. These wires were then converted to Te or Bi_2Te_3 by a galvanic displacement reaction in which either Te or Bi_2Te_3 are deposited during a concomitant oxidant-mediated dissolution of the Ni-Cu nanowires, as shown in figure 19.

Additional semiconductor materials have been templated using DNA. Dittmer and Simmel templated λ -DNA with CuS in both solution and on a substrate using CuCl_2 reacted with either Na_2S or HS respectively.⁴¹ AFM and TEM revealed single DNA strands templated with CuS NPs less than 10 nm in diameter with a 40 nm inter-particle spacing. However, the use of bundled DNA strands increased NP density by an undefined value to generate more continuous structures. This was due to an increased number of nucleation sites as a higher density of binding sites were available for the copper ions. Li et al templated BaWO_4 onto *E. coli* genomic DNA by reacting $\text{Ba}(\text{NO}_3)_2$ with Na_2WO_4 in solution.¹¹ Interestingly, two parallel nanowires were formed through the thermal denaturation, and consequential unravelling of the dsDNA.

Lastly, Kundu et al uniquely synthesised continuous CdS nanowires 140 - 170 nm in diameter and 8 - 12 μm in length through incubating

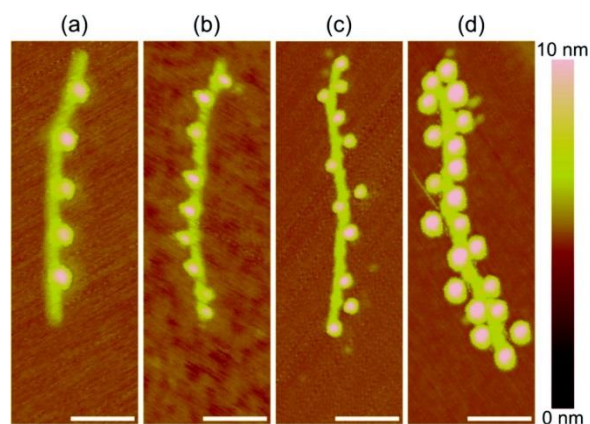


Figure 20: AFM images of streptavidin-conjugated QDs attached to functionalized DNA origami nanotubes with (a) 5 binding sites (71 nm period); (b) 9 binding sites (43 nm period) (c) 15 binding sites, (29 nm period); and (d) 29 binding sites (14 nm period) (scale bars = 100 nm). Reprinted with permission from *Nano Lett.*, 2010, **10**, 3367. Copyright 2010 American Chemical Society.

λ -DNA with cadmium perchlorate, and thioacetamide in the presence of microwave radiation for 60 seconds.⁶⁴

2.4.6 Discrete Semiconductor Structures. Bui et al generated a linear array of streptavidin-conjugated quantum dots (QD) on a DNA origami template.²⁵ The template consisted of six helix bundles (412 nm in length and 6 nm in diameter) containing selected extended thymine staple strand chains (2.2 nm in length) modified with biotin at the 3' end. Through varying the number of biotin staple strands; various QD periodicities could be programmed: 5, 9, 15, and 29 biotin attachment sites gave QD periodicities of 71, 43, 29, and 14 nm, respectively, as shown in figure 20. However, not all binding sites were utilised when 15 and 29 biotin sites were available. The authors suggest this may be due to (i) steric hindrance between QDs; (ii) QDs occupying multiple binding sites; and (iii) missing or compromised biotin staple strands.

Torimoto et al used positively charged CdS NPs that were electrostatically adsorbed to dsDNA (isolated from salmon testes) to form discrete structures 3 nm in diameter, with an inter-particle spacing of 3.5 nm.⁶⁵ A similar electrostatic interaction was exploited by Artemyev et al in which CdSe/ZnS core-shell nanorods (4.5 nm x 25 nm) were templated onto λ -DNA to form linear structures greater than 1 μm in length and less than 100 nm in width.⁶⁶ Stsiapura et al formed highly ordered quasi-nanowires by incubating positively charged CdSe/ZnS QDs (4.8 nm) and rods (4 nm x 25 nm) at different stoichiometric ratios with λ -DNA prior to combing onto coverslips: the average quasi-nanowire length of stretched DNA was $17.6 \pm 1.2 \mu\text{m}$.⁶⁷

2.4.7 Biomolecules. In addition to the use of biotin-modified DNA templates to direct self-assembly of streptavidin-coated NPs (section 2.4.2), additional biomolecules have been utilised. For example, histidine-tagged protein was demonstrated to reversibly bind to Ni^{2+} -DNA complexes and λ -DNA-templated Ni metal. The authors

suggest this could provide a means to produce high-density protein assemblies for proteomic analysis.⁶⁸ Nishinaka et al produced a template consisting of the RecA protein, containing a modified reactive amino acid residue, wrapped around a DNA strand.⁶⁹ RecA provides a higher mechanical stiffness and stability compared to dsDNA alone. Functionalised Au NPs attached to the modified amino acid, and a subsequent metallisation step produced uniform continuous nanowires. Recently Ruff et al utilised a linear or circle dsDNA to template the assembly of filamentous virus-like particles into 1D structures.⁷⁰ The monomers consisted of 'mushroom-shaped' nanostructures of coiled-coil peptides with cationic segments for DNA attachment at one terminus, and PEG chains for water solubility at the other.

3. Characterisation and Properties

An essential step in the development of any nano-scale device is its characterisation. This is not only to determine if the synthesis or manufacturing process proceeded correctly, but also, and perhaps more importantly, to investigate the properties of the device, which might then suggest suitable applications. This section will outline some commonly applied methods for the study of DNA-templated structures, first briefly commenting on sequencing of the DNA template itself before moving on to imaging and microscopy techniques, and then discussing more detailed electrical and spectroscopic characterisation.

3.1 Sequencing

If the DNA template relies on the specific order of its nucleotides, it is important to check that these have been synthesised correctly by sequencing the DNA before proceeding further. Historically, DNA sequencing is an enzymatic process in which a template is replicated in solution by DNA polymerase to create a large enough sample size. This allows analysis techniques such as well-established polyacrylamide gel electrophoresis,⁷¹ or the more advanced Next Generation Sequencing (NGS) technique of pyrosequencing where solutions of individual nucleotides are added sequentially to a single stranded template.⁷² If the added nucleotide complements the first unpaired base, pyrophosphate (PPi) is released as the DNA polymerase facilitates the base pairing. The PPi is then detected by light released from a chemiluminescent enzymatic reaction. Other NGS techniques exist that focus on high throughput and low cost by parallel processing, with commercial pyrosequencing systems capable of sequencing nearly 14,000 base pairs per second.⁷³ However, a major common disadvantage is their requirement for large sample sizes, and often requiring unzipping the DNA template into single strands.

For the envisioned nano-scale applications of DNA-templated structures, very few, or even single molecule devices are fabricated. It would therefore be ideal to be able to sequence the same single DNA molecule that would form the template, rather than relying on enzymatic duplication. Any modification

of the template, by unzipping or otherwise, is also to be avoided. To this end, several 'third generation' sequencing techniques are being developed, such as identifying electron tunnelling characteristics through each base pair as the DNA molecule passes through a nanopore.⁷⁴ This is a direct and completely non-destructive technique, although it is currently limited to low throughput with a potential sequencing rate of just tens of base pairs per second. However, this has not yet been enhanced by any parallel processing, which is the source of the orders-of-magnitude higher sequencing rate in current NGS systems.

3.2 Imaging

Imaging is the most fundamental characterisation technique, instantly giving vital morphological and conformational information. Indirect imaging or other structural analysis, such as crystallography and scattering techniques, most often require an artificial, macroscopic crystalline sample. This is possible to achieve with 3D DNA self-assembly,⁷⁵ however, this is not suitable for analysing small quantities, or especially single molecules, and precludes the study of structures in any non-crystalline environment. This makes these techniques inappropriate for imaging isolated 1D structures, although spectroscopy is still used for chemical characterisation, which will be discussed in section 3.4.

Direct imaging techniques, such as optical microscopy, Scanning Probe Microscopy (SPM) or Electron Microscopy (EM), provide more convenient analysis methods, enabling simple characterisation of almost any structure in a wide variety of environments. Imaging most often complements other analysis techniques in confirming suspected properties.

3.2.1 Optical microscopy. As a nanometre scale structure, and hence far below the wavelength of visible light, DNA and its templated structures may seem impractical for analysis by optical microscopy. The Abbe diffraction limit gives the minimum resolution as $\lambda/(2NA)$, where λ is the wavelength of light and NA is the numerical aperture of the objective.⁷⁶ Visible light microscopes are hence unable to resolve separate features closer than approximately 200 nm apart. However, for sufficiently well-spaced structures of a large enough scale, fluorescence microscopy is commonly used. A number of techniques are also in development for pushing back the boundaries of the diffraction limit.

Fluorescence is an optical phenomenon whereby an excited orbital electron in an atom or molecule relaxes to a lower energy state, emitting a photon of a characteristic wavelength. The excitation is achieved via absorption of light of a slightly different wavelength, provided by a laser. Fluorescent molecules, known as fluorophores, are used as dyes, binding to certain target molecules and revealing their position. A particularly relevant dye for dsDNA, which would not otherwise fluoresce, is a compound known as YOYO-1, a tetracationic homodimer of Oxazole Yellow.^{29, 36, 77, 78} This



Figure 21: Fluorescence microscopy image of DNA strands, dyed with YOYO-1. Scale bar = 300 μm . Reprinted with permission from *ACS Nano*, 2013, 7, 4326. Copyright 2013 American Chemical Society.

may be used to check the position and conformation of a DNA template before it is seeded with the desired material. An example can be seen in figure 21.

The majority of DNA-templated structures that are examined by fluorescence microscopy make use of the fluorescence of the templated material itself, where available, rather than binding other fluorophores to the DNA molecule. As bare DNA does not fluoresce, this aids in confirming that the templating process has succeeded.

Overcoming the wavelength limit of visible light poses a key challenge for high-resolution imaging using the convenience of direct optics. A recent review describes these 'super-resolution' techniques, or 'nanoscopy', as utilising selective switching of fluorophores.⁷⁶ Stochastic reconstruction techniques are used based on time-resolved monitoring of the on/off behaviour of fluorophores. In 2010, Jungmann et al demonstrated DNA-Point Accumulation for Imaging in Nanoscale Topography (DNA-PAINT), where short fluorescent oligonucleotides (imager strands) in solution transiently bind to complimentary 'docking' strands on the surface-immobilised template. The system was studied in a Total Internal Reflection Fluorescence Microscope (TIRFM), where the surface-localised nature of the excitation light only allowed bound fluorophores to actually fluoresce. A blinking of the intensity was thus observed as the imager strands interacted with the docking strands. Altering the lengths and concentration of the imager strands allowed control over the duty cycle. This enabled statistical averaging of

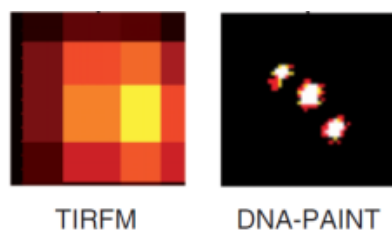


Figure 22: Comparison of TIRFM image and the super-resolution DNA-PAINT technique, where three fluorophore binding sites on a DNA template are clearly resolved. Reprinted with permission from *Nano Lett.*, 2010, 10, 4756. Copyright 2010 American Chemical Society.

the blinks, defining areas of higher intensity, and allowing the positions of the docking strands on the template to be successfully resolved, with a separation of ~ 130 nm.⁷⁹ A comparison of standard TIRFM and DNA-PAINT can be seen in figure 22.

3.2.2 Atomic Force Microscopy (AFM). SPM techniques are widely used for their nano-scale resolution. Scanning Tunnelling Microscopy (STM), although capable of atomic resolution, is limited to conductive samples, and therefore not suitable for analysing many biological materials, such as DNA.

In contrast, AFM relies only on the intermolecular forces between the tip and the sample, where the tip is mounted on the end of a flexible cantilever. As the tip is scanned across the surface, the topography is mapped out by monitoring the deflection of the cantilever. As such, one of the major advantages of AFM over the other imaging techniques discussed here is that it provides 3D information. Typically the vertical resolution is an order of magnitude better than the lateral resolution.^{29, 77}

As with other SPM techniques, the lateral resolution is limited only by the diameter of the tip. The finite diameter introduces a convolution effect where the edge of the tip meets a feature before the centre point, causing the cantilever to be displaced early.⁵⁶ This systematic error may be corrected for by calibration against a sample of known dimensions. This is essential for quantitative height profiling, however, it is rarely carried out, leading to a mismatch between reported height and width values for structures which could be expected to have a circular cross-section.^{29, 77} In general, it is the height values which are to be trusted from AFM. Metallic structures templated on single DNA molecules exhibit heights in the range of 3 - 23 nm, depending on the diameter of the NPs used to seed the template.^{48, 63, 77, 80} For the three helix bundle template synthesised by Park et al, AFM measured an accordingly greater height of 27 nm.¹⁶

For soft, organic samples, scanning with the tip in contact with the surface, known as 'contact mode', often damages the sample.⁷⁶ To avoid this, the cantilever may be oscillated near its resonant frequency such that the tip only makes contact with the surface at its maximum displacement. This is known as 'intermittent contact mode', or tapping mode, and reduces the lateral contact forces inflicted on the sample. This mode is used almost exclusively for analysing DNA-templated samples. The perpendicular contact forces may however deform soft materials, introducing further discrepancies between lateral and vertical measurements.^{48, 56} Measured heights of organic polymer structures templated on single DNA molecules are smaller than those of metallic structures, being in the range of 1 - 7 nm.^{55, 56, 81} Hassanien et al observed that their strands of polyindole-DNA aggregated in solution to form rope-like structures.¹¹ This was attributed to the polymer compensating for the otherwise mutually repulsive charge on the DNA, which has also been reported for other polymers.⁵⁶ The result was a

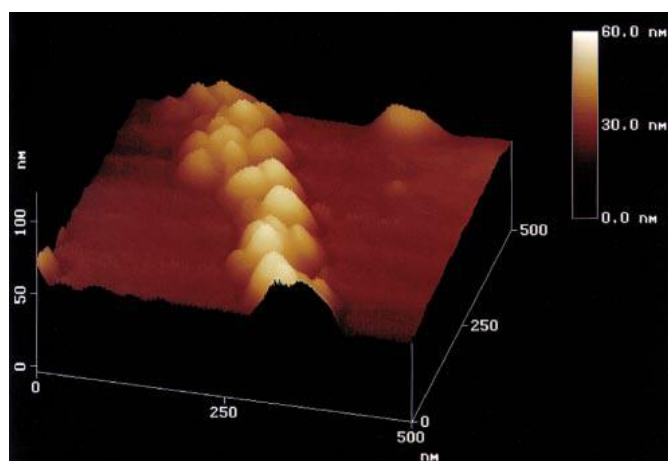


Figure 23: 3D AFM image of Ag aggregates on a DNA template. Reprinted by permission from Macmillan Publishers Ltd: *Nature*, **391**, 775, copyright 1998.

comparatively large magnitude and variation of height, ranging from 5 - 33 nm. This aggregation is not observed with templates fixed to a surface.⁵⁶

AFM can be easily applied to a wide variety of systems in ambient conditions with minimal preparation. This includes imaging in liquid environments such as buffer solutions, which is especially advantageous for biological samples, as it can allow control of factors such as pH, and mimic native conditions for DNA.⁷⁶ As such, AFM has become one of the most widely used methods for imaging DNA-templated structures, and examples can be found in most experimental papers.

Early work by Braun et al involved the deposition of Ag ions on a fixed DNA template.³⁶ The reduction and development process used to aggregate the Ag into a continuous structure resulted instead in a large, highly non-uniform, granular structure, 100 nm wide and 12 μm long, part of which can be seen in figure 23. This granularity suggests a possible cause for the unusual electronic properties, which will be discussed in section 3.3.

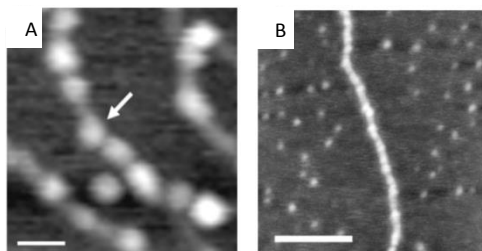


Figure 24: AFM images of CdS NPs on a DNA template. (A) Discrete NPs (white arrow) on fixed template. Height scale = 5 nm, scale bar = 25 nm. (B) Smoother structure templated in solution. Height scale = 3 nm, scale bar = 100 nm. Reprinted with permission from *Adv. Mater.*, 2007, **19**, 1748, ©2007 Wiley-VCH Verlag GmbH & Co. KGaA, Weinheim.

In an extension of this, AFM can reveal the quality of any metallisation process, easily distinguishing between incomplete, 'beads-on-a-string' and smooth structures, two results which give rise to completely different properties. This allows the synthesis and reaction conditions to be optimised, and significantly smaller and smoother structures have now been fabricated. A comparison of these morphologies is shown in figure 24, produced by templating CdS NPs. Structures formed by combining the DNA templates and CdS NPs in solution show a far more continuous coverage than structures formed by depositing the NPs on fixed templates.⁶³ This difference in coverage has also been found for other materials.^{55, 82}

3.2.3 Electron Microscopy (EM). Exploiting wave-particle duality allows one to exceed the diffraction limit of visible light without resorting to shorter wavelengths of electromagnetic radiation, which become increasingly difficult to produce and manipulate. The de-Broglie wavelength of the electrons used gives a theoretical resolution of approximately

1 nm.⁷⁶ This makes EM ideal for studying DNA-templated structures, which have important nanoscale features. However, sample preparation is elaborate, and the high vacuum required for the electron beam precludes native conditions. Due to its high resolution and lack of any tip convolution effects, EM is commonly used for estimating in-plane dimensions, which are largely material-dependent for DNA-templated structures, ranging from lengths of several microns to widths of 1 - 100 nm.⁸² The two main types of EM are SEM and TEM.

A SEM system consists of a focussed electron beam which is scanned across the sample surface. Back-scattered electrons are then collected and recorded at each pixel. Practical resolutions are limited by the aberration factors introduced by the magnetic

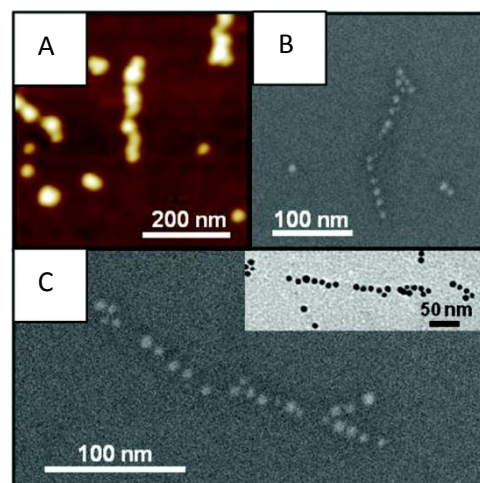


Figure 25: Au NPs seeded on a DNA template. (A) AFM image, height scale = 20 nm. (B) and (C), example SEM images, revealing separation between NPs. Inset shows a brightfield TEM image of a similar structure. Reprinted with permission from *J. Phys. Chem. B*, 2012, **116**, 10551. Copyright 2012 American Chemical Society.

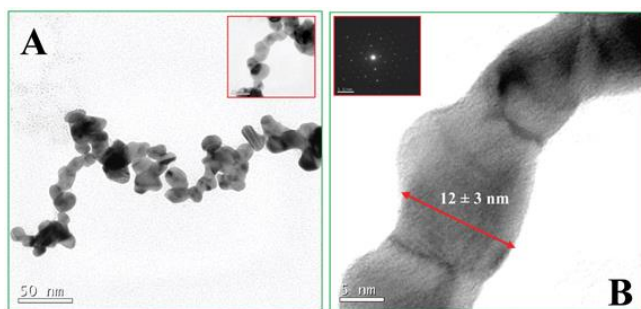


Figure 26: TEM images of Au NPs aggregated on a DNA template. (A) Low magnification image. (B) High magnification image. Inset of (B) shows SAED pattern taken from the area shown in the inset of (A).¹⁴

lenses, which affects the spot size of the electron beam. Non-conductive samples must be metallised to prevent charge build-up at the surface, which may also obscure the finer features. Figure 25 shows a comparison of AFM and EM images of discrete Au NPs seeded on a DNA template.¹⁵ The greater resolution of SEM allows the separation between NPs to be observed, which is obscured in AFM. Despite its complexity, nanometre resolutions are still feasible for SEM.⁷⁶ Although its applications in studying DNA-templated structures are limited to conductive materials, many examples are available due to the high level of interest in fabricating self-assembled conductive structures, which will be discussed in section 3.3.^{15, 16, 38, 83, 84}

In contrast to the focussed electron beam used in SEM, TEM uses a diffuse electron beam which impinges upon the entire sample. Electrons which are transmitted through the sample are collected by a CCD detector placed underneath. This requires very thin samples no thicker than the order of 100 nm, which is rarely a limitation for 1D DNA-templated structures. Although TEM is also a complicated process, and still limited to high vacuum, 0.1 nm resolution is possible with electrons accelerated to 100 - 200 kV.⁷⁶ This makes it particularly popular for assessing the finer detail of 1D arrays of NPs templated on DNA, such as the Au NPs shown in figure 26, where the resolution of AFM, or even SEM, may not be sufficient.¹⁴ Quantitative dimensional measurements can be made, and analysis of the Selected Area Electron Diffraction (SAED) pattern also reveals crystallographic information. The example shown in the inset of figure 26b indicates the Au NPs are single crystalline.

3.3 Electronic

A large fraction of 1D DNA-templated materials are constructed for the purpose of conducting electricity, with a view to assembling nano-scale circuits and devices. Due to the negligible long-range conductivity of pure DNA,^{38, 56, 81, 82} a wide variety of materials have been investigated as templating options for enhancing the conductivity, from metals and inorganic compounds to semi-conducting, organic polymers. Understanding the electrical conductivity and transport properties of these various nanowires is essential, although

through electronic characterisation of materials reported as nanowires does not always take place.

The vast majority of electronic studies simply measure the conductivity of a nanowire. However, DNA-templated structures are very versatile, and, by site-specific attachment, are not limited to one material only. The potential novel electronic properties of these structures have yet to be thoroughly explored. In particular, hybrid combinations of organic and inorganic materials are especially interesting. Wang et al studied binary nanowires consisting of regularly spaced Au NPs interspersed with stretches of polyaniline.⁸¹ The organic polymer acted as a barrier between the NPs, creating a series of tunnel junctions along the template. This allowed analysis of the Coulomb blockade effect and its dependence on junction number, an important step for the development of single electron devices.

Two main electrical characterisation methods exist: two terminal measurements and conductive AFM.

3.3.1 Two Terminal Measurements. The majority of electrical measurements carried out on DNA-templated nanowires take place between two micro-fabricated electrodes, easily constructed with standard photolithography or electron-beam lithography methods, usually consisting of recessed Au contacts patterned into a SiO₂ substrate, giving a level surface overall. A recent review highlights the possibility of leakage current through the substrate due to water condensation on the dielectric.⁸⁵ This may be minimised by operating in a dry atmosphere. The set-up allows simple yet versatile measurements to be carried out on a wide variety of materials, yielding characteristic Current-Voltage (I-V) curves.^{15, 16, 36, 38, 56, 63, 83}

Alignment of the nanowires across the terminals may be achieved by the methods described in section 2, most commonly via the receding meniscus, molecular combing technique.^{38, 56, 63}

Measurements on single nanowires are more common, however, measurements may also be carried out on two-dimensional arrays of multiple, aligned nanowires, which can give statistical advantages with large sample sizes. Ma et al demonstrated controllable conductance of an array of stretched, immobilized DNA strands coated in polyaniline.⁵⁶ In its intrinsic form, polyaniline is an insulator, however, introducing HCl vapour protonated the polyaniline, creating mobile charges balanced by the Chloride counterions. This raised the conductance of the nanowire array from negligible to approximately 30 nS. The doping process was reversed by introducing NH₃ gas, which deprotonated the nanowires, causing the conductance of the array to decrease to its original value.

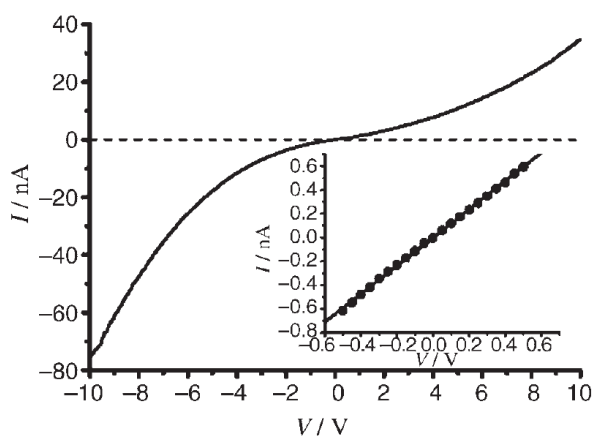


Figure 27: IV Curve of polypyrrole-DNA nanowire. Inset shows ohmic behaviour at low bias corresponding to a resistance of 843 Ω . Reprinted with permission from *Chemistry*, 2007, **13**, 822, ©2007 Wiley-VCH Verlag GmbH & Co. KGaA, Weinheim.

Single nanowire measurements are more significant for the development of nano-scale electronic components. Braun et al constructed their Ag nanowire on a DNA template fixed between two terminals.³⁶ The measured I-V curve showed a zero-current plateau at low bias. A suggested possible cause for this non-ohmic behaviour was the granular nature of the nanowire, revealed by AFM images. This exemplifies how multiple characterisation techniques may complement each other.

Synthesis methods have since improved, with increasingly smoother nanowires of both organic and inorganic materials being fabricated, confirmed by various imaging techniques. An I-V curve measured across a polypyrrole-DNA nanowire is shown in figure 27, with the inset showing ohmic behaviour at low bias corresponding to a resistance of 843 Ω . The non-linear behaviour is typical of Schottky energy barriers formed at the interface between the semiconducting

nanowire and metallic electrode.⁵⁵ This does not affect metallic nanowires, which exhibit ohmic behaviour across a much larger range of bias voltages.^{15, 16, 38, 83} In general, metallic nanowires exhibit orders of magnitude higher conductivity, ranging from 1600 – 20000 Scm^{-1} , than conducting polymer nanowires, which range from 4 – 40 Scm^{-1} .^{11, 55} Despite this, conducting polymers are still of interest due to the wider range of chemistries and functionalization options available.

Two terminal systems are ideal for investigating environmental variations, such as the acid/base doping discussed above, and also thermal variations, which would be expected to affect conductivity. Hassanien et al measured I-V curves of polyindole-DNA nanowires from 233 – 373 K, finding an increase in conductivity with increasing temperature. This was the expected thermally activated Arrhenius temperature dependence for charge hopping along the polymer.¹¹ The conductance of metallic nanowires has also been found to increase with temperature, consistent with their granular nature.⁸⁶

Despite its simplicity and versatility, one unavoidable drawback of two terminal systems is the inclusion of the nanowire-electrode contact resistance. This increases the total measured resistance, making it difficult to quantify the exact contribution of the nanowire.

3.3.2 Conductive AFM (c-AFM). An alternative electronic characterisation approach makes use of an AFM modified with a conductive tip. By using drop-casting, molecular combing techniques, a sample of nanowires may be prepared such that single nanowires extend radially from a bulk agglomeration.^{11, 48, 82} A macroscopic contact can be made at the bulk material, and the AFM tip may be positioned on a nanowire to make the second contact. The effective length of the nanowire can therefore be varied as the tip is moved. Extrapolating the

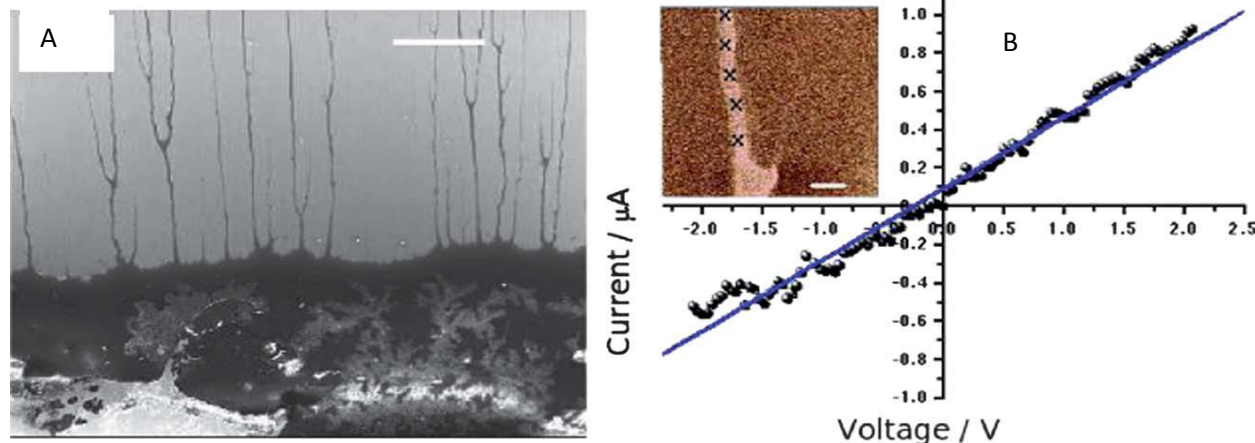


Figure 28: Conductive AFM measurements on Pd nanowires. (A) SEM image of nanowires extending from bulk. Scale bar = 20 μm . (B) Example I-V curve. Inset shows conductive AFM image marked with locations of I-V measurements. Data scale = 500 nA, sample/tip bias = 5 V, scale bar = 1 μm .⁸⁴

conductance – length plot to zero length provides a baseline contact resistance, allowing the contribution of the nanowire to be isolated. An example c-AFM set-up can be seen in figure 28, which shows a SEM image of individual nanowires extending from the dried droplet of bulk material in figure 28a, and a typical I-V curve in figure 28b, where the inset shows the positions along the wire where measurements were taken.⁸⁶ The I-V curve is approximately linear, reflecting the metallic nature of the Pd nanowires, the conductivity of which was measured as 1600 Scm^{-1} .

By holding the surface at a potential difference relative to the tip and scanning at a fixed displacement from the surface, typically 50 nm, the phase of an oscillating c-AFM tip will be sensitive to the local electric field, mapping the conductivity as seen in the inset in Figure 28b. This technique allows qualitative electrical characterisation, and is known as Scanning Conductance Microscopy (SCM) or Electrostatic Force Microscopy (EFM).⁴⁸ Due to the low capacitance between the nanowire and the substrate, it is sensitive even to nanowires with low conductivity.⁸⁵ Most commercial AFM systems are easy to adapt for this relatively simple technique, making it a good choice for rapid, qualitative, initial characterisation.

c-AFM is not without its complications. A higher tip contact force systematically reduces the measured resistance due to increased deformation and contact surface area. This indicates that the nano-scale tip-nanowire contact resistance is the dominant source of contact resistance in the system, although its variation is not fully understood.^{48, 86}

3.4 Spectroscopy

A variety of spectroscopies may be used for chemical characterisation of DNA-templated materials. Most commonly these are carried out to not only verify the presence of the target material, such as with Energy-dispersive X-Ray spectroscopy (EDS) and X-Ray Photoelectron Spectroscopy (XPS), but critically to also investigate its bonding to the template, such as with Fourier-Transform Infrared Spectroscopy (FTIR). Spectroscopy in the UV-Visible range (UV-Vis) can also reveal some interesting optical properties of 1D DNA-templated structures.

3.4.1 EDS and XPS. EDS spectra consist of the secondary X-Rays emitted when an outer orbital electron relaxes to fill the lower energy state left by an ejected inner orbital electron. Each element has characteristic wavelengths associated with its atomic energy levels, allowing simple elemental identification. The ionising energy is typically supplied by a beam of accelerated particles, making it possible to be conveniently collected simultaneously with TEM.^{14, 86, 87} XPS works via the same principle in reverse, ie. measuring the energies of emitted electrons when the sample is irradiated with X-Rays. It is also sensitive to oxidation states, allowing observations of oxidation reactions of the templated material due to ambient conditions. EDS and XPS complement each other, and may be used as reference checks.^{14, 86}

3.4.2 X-Ray Diffraction (XRD). XRD is a crystallography technique used for determining the structure of crystalline materials with up to atomic resolution. This is best suited for inorganic templated materials with some periodicity, whether by design for discrete structures or due to aggregation during the metallisation process of continuous structures. Its resolution is indicative of the crystalline quality of the sample, and may allow quantification of the crystal orientation and/or lattice parameter.^{14, 86, 87} This aids in the analysis of unusual electronic properties, which are often caused by grain boundaries in nanowires.

3.4.3 Small Angle X-Ray Scattering (SAXS). SAXS also provides morphological characterisation of nano-scale structures, yet does not require a crystalline sample. Vial et al used SAXS to analyse complex hybrid chains of Au nanorods linked by multiple DNA strands, resulting in side-by-side alignment of the nanorods, creating ladder-like ribbons.⁸⁴ The measured periodicity verified SEM observations. The self-assembly process was monitored by SAXS, which revealed three phases of development, termed ribbon growth, ribbon stacking from 2 - 48 hours, consisting of randomly orientated layers, and registered stacking from 48 hours onwards, where the layers became increasingly aligned. This represents an important step in understanding the dynamic development of hierarchically self-assembled structures.

3.4.4 FTIR. FTIR collects spectroscopic data over a broad range of wavelengths, making it a very versatile technique. Typically the absorbance is recorded, ie. the relative decrease in intensity of light passed through the sample.⁸⁶ The inverse parameter, transmission, also provides similar data.¹⁴ The spectra are characteristic of the molecular energy levels present due to bond vibrations, hence small shifts are observed when the chemical composition is altered. This is especially useful for characterising the bonding of a material to its DNA template, which directly confirms the interaction and templating process.

3.4.5 Surface Enhanced Raman Scattering (SERS). Raman Scattering is a spectroscopic technique based on detecting the small characteristic shifts in energies of photons scattered inelastically from orbital electrons. However, the majority of photons scatter elastically, and hence the shift is a very weak effect. SERS amplifies this effect by placing the sample on a rough metallic substrate, allowing increased charge oscillation and analysis of smaller sample sizes. Kundu et al recently investigated the SERS Enhancement Factor (EF) of a 1D, DNA-templated Au substrate, carrying out a test measurement on a standard fluorescent dye, R6G.¹⁴ An EF of approximately 10^6 was found, comparable with other studies and systems. These Au structures were found to have stable optical properties after 6 months, indicating the possibility of long-term applications.

3.4.6 UV-Vis. UV-Vis Absorption spectra have been measured for a variety of DNA-templated materials, which are again used to assess the self-assembled chemical structures against known standards. Chen et al verified the polymerisation of monomers along their template by observing a UV-Vis spectra typical of conducting polymers.⁸⁸ Vial et al were also able to monitor the self-assembly process in solution via observing the changes in the UV-Vis spectra, which confirmed that self-assembly was taking place in the mixture of nanorods and DNA linking strands.⁸⁴

Rather than simply using UV-Vis spectroscopy as a characterisation tool, other studies make more of a step towards potential optical applications. Sezi et al report the enhanced absorption of solutions of ethynyl pyrene chromophores when self-assembled onto complementary ssDNA templates.⁸⁹ The DNA remains in aqueous solution while the excess chromophores precipitate out. An estimated 12 chromophores were templated onto each 17 bp long DNA strand, whilst a control experiment with a non-complementary template, allowing only covalent bonding, retained only up to 5 chromophores per DNA strand. The greater number of chromophores in solution therefore led to the enhanced absorption at the characteristic frequencies of the dye. In contrast to this enhancement of optical properties, Galievsky et al report quenching of the fluorescence of pyrenedicarboxamide building blocks incorporated into both SS and dsDNA.⁹⁰ This was attributed to electron transfer reactions with the neighbouring bases. The fact that the optical properties of various materials may be selectively enhanced or suppressed demonstrates the versatility of DNA templating.

4. Applications

An important consideration for any field of research is practical application and how novel methods could be used to improve existing technology or create brand new technologies where previous limitations had deemed them impossible. DNA-templated technology is a growing field of research and novel applications are being continually developed. This section will provide a varied outline of current applications for DNA-templated technology, including nano-electronics, biosensing and thin film applications. The featured examples highlight current areas of research, demonstrating the flexibility and potential of DNA templating.

4.1 Conductive Nanowires

The construction of nanometre scale circuits is problematic due to difficulties of achieving inter-element wiring and creating electrical interfaces on macroscopic electrodes.³⁶ Molecular recognition and the self-assembly of molecules into supramolecular structures could potentially be used to overcome these challenges. DNA has the appropriate molecular recognition and mechanical properties to fill this role, but poor conductivity prevents pure DNA from being directly useful in electrical circuits.^{38, 91} Despite this setback, many inventive

ways of using DNA have been developed which are able to improve its conductivity, opening up its potential in the electronics industry.

One of the first DNA-based conductive nanowires was produced by Braun et al. They demonstrated a technique for producing conductive Ag nanowires connected between two electrodes using DNA as a template.³⁶ This technique involved two steps, the self-assembly of a DNA bridge between two electrodes and the vectoral chemical deposition of Ag onto the DNA bridge, resulting in a Ag coated DNA-templated nanowire. The wires produced in this study were found to have a high resistance of ~30 M Ω and diameters up to ~100 nm. The wet chemistry approach which was introduced by Braun et al has since been used to create DNA-templated nanowires out of Au⁹², Pt,⁹³ Pd⁹⁴ and Cu.⁹⁵ The drawback of wires which are metallized in this manner is that they are prone to having granular metal deposition sites and become highly resistive at low temperatures.⁹⁶

A dry deposition method which overcomes the low temperature resistance issue is to sputter a thin metallic film on DNA strands when they are suspended between two electrodes. Hopkins et al used this method to create superconducting Mo₂Ge₇₉ nanowires with diameters as thin as 5 – 15 nm. The resulting wires demonstrated superconducting behaviour at low temperatures below 2 K.⁹⁶

DNA can be enhanced by the addition of proteins. A study by Nishinaka et al⁶⁹ has demonstrated nucleoprotein filaments constructed by binding RecA proteins to a double stranded DNA template. The resulting nucleoprotein filaments were found to have a higher degree of stiffness compared to dsDNA, providing a robust scaffold for well organised electrical circuitry at the nanometre scale. Using sequence specific protein patterning, it is possible to control the metallization of the filament, allowing for the creation of both conductive and non-conductive regions.

Park et al have demonstrated another method for creating 1D Ag nanowires using three-helix bundles of DNA as mentioned in section 2.¹⁶ These bundles consist of three double helical DNA domains connected by six immobile crossover junctions arranged in a way that prevents the helix axes from being coplanar. These can produce 1D filaments or 2D lattices. The 1D filaments were metallized with Ag, forming uniform wires with an average width of 30 nm and a resistance of ~1.2 k Ω . This is 25,000 times lower than the resistance of Ag nanowires originally produced by Braun et al³⁶ and represents a large step towards producing uniform, low resistance DNA-templated nanowires.

Conducting polyaniline nanowires were originally fabricated by Ma et al by using fully stretched DNA as a growing template while applying a gentle HRP enzymatic polymerisation approach.⁵⁶ A different photo-polymerisation approach to produce similar polyaniline nanowires and Au NP – polyaniline alternated hybrid nanowires has also been studied by Wang et al.⁶⁰ These polyaniline nanowires demonstrated Schottky emission dominated conduction and a rectification effect. These wires could have applications in

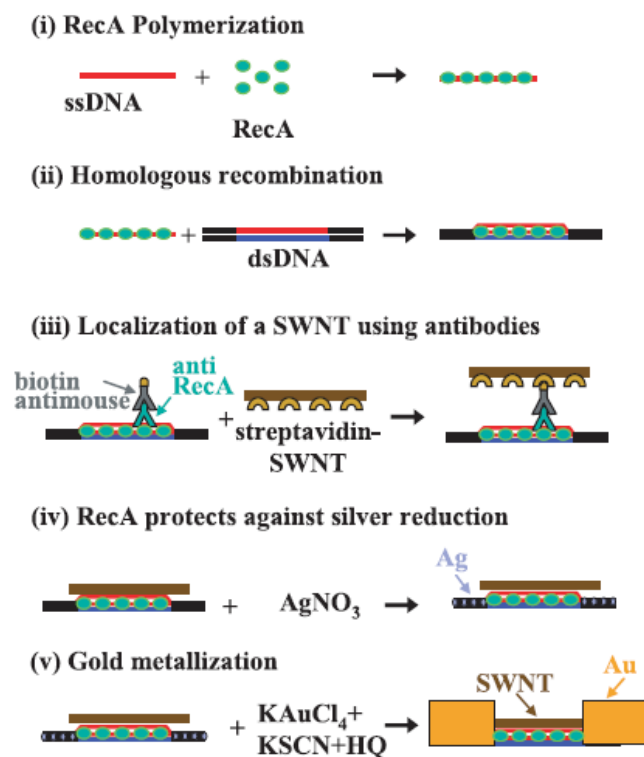


Figure 29: The process used by Keren et al to produce DNA-templated carbon nanotube FETs. (i) RecA polymerisation of ssDNA to form nucleoprotein filaments. (ii) Recombination reaction. (iii) Antibody based localization of SWNT. (iv) Incubation in AgNO_3 solution. (v) Electroless Au deposition. From *Science*, DNA-templated carbon nanotube field-effect transistor, **302**, 2003, 1380-1382, Kinneret Keren, Rotem S. Berman, Evgeny Buchstab, Uri Sivan and Erez Braun, figure 1. Reprinted with permission from AAAS.

diode construction. The Au NP-polyaniline wires demonstrated Coulomb blockade effects.

The application of DNA-templated nanowires is a new field, but there are examples which help to demonstrate their potential in nano-scale electronics.

Keren et al⁴⁴ have used DNA molecules to connect semiconducting single walled carbon nanotubes (SWNT) together and then act as a template to create metallised conducting nanowires between the SWNTs. Using this method, they have produced DNA-templated carbon nanotube Field Effect Transistors (FET), capable of operating at room temperature. To produce this device, the process developed by Nishinaka et al⁶⁹ has been used. This involved binding RecA monomers polymerised on a ssDNA molecule to form a nucleoprotein filament. A homologous recombination reaction binds the nucleoprotein filament at the desired address on an aldehyde-derivatised scaffold dsDNA molecule. The DNA-bound RecA is used to localize a streptavidin-functionalised SWNT, using a primary antibody to bind a RecA protein and a biotin-conjugated secondary antibody. Incubation in a AgNO_3 solution leads to the

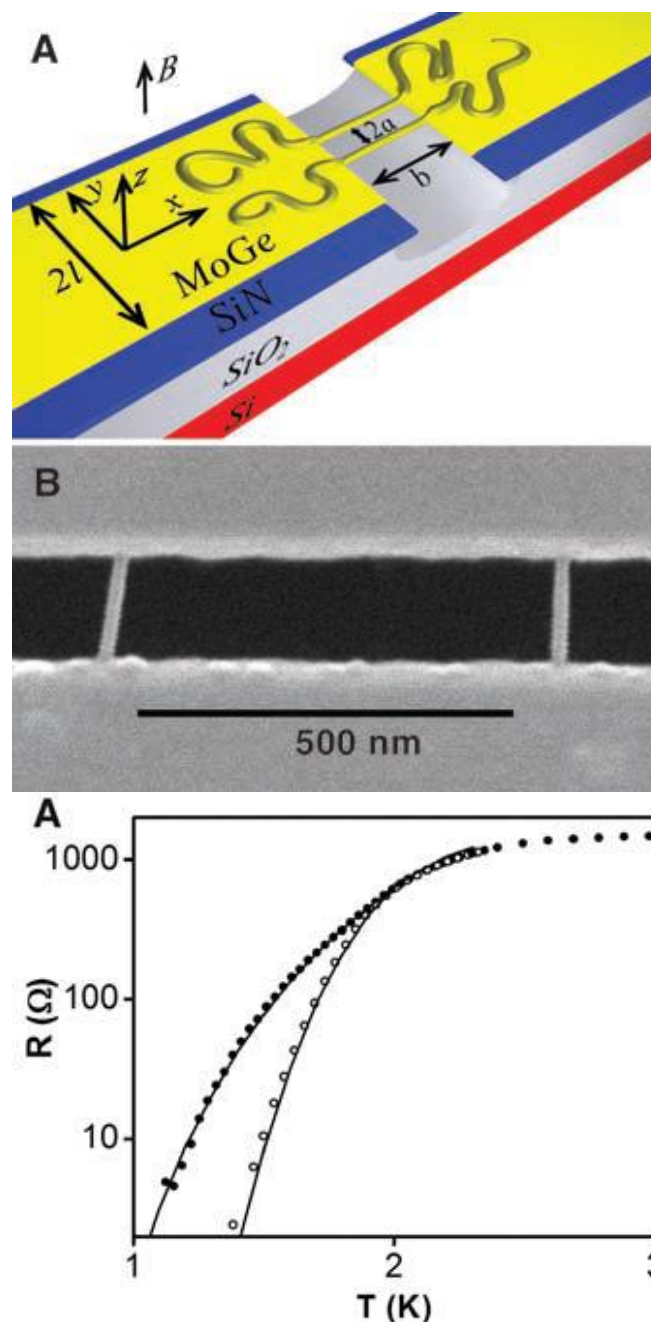


Figure 30: (A) A schematic image of the quantum interference device, two DNA strands are stretched across a SiN/SiO₂ trench and sputtered with superconducting Mo₂₁Ge₇₉. (B) SEM image of two metal coated DNA molecules. (C) Resistance vs temperature graph demonstrating the difference between no magnetic field (blank circles) and an applied field of 228 μT (solid circles). From *Science*, Quantum interference device made by DNA templating of superconducting nanowires, **308**, 2005, 1762-1765, David S. Hopkins, David Pekker, Paul M. Goldbart and Alexey Bezryadin, figures 1 and 2. Reprinted with permission from AAAS.

formation of Ag clusters on the segments that are unprotected by RecA. Electroless Au deposition is then used to coat the Ag clusters, resulting in the formation of two DNA-templated Au wires

contacting the SWNT at both ends. The process is shown in figure 29. This process created devices with a single SWNT or a rope of them bound together; however the bound rope devices do not exhibit FET behaviour. This could be due to the inclusion of conducting SWNTs amongst the semiconducting ones.

Superconducting DNA-templated nanowires have been used to produce quantum interference devices, as demonstrated by Hopkins et al.⁹⁶ In the study, two DNA strands were stretched across a trench which had been etched into SiN/SiO₂ on a Si chip.³⁸ The molecules and banks are then coated with superconducting Mo₂₁Ge₇₉ using dry sputtering. This is shown in figure 30. Below 2 K the wires became superconducting and their resistance dropped off exponentially. The resistance changed with an applied magnetic field at these temperatures. As a result, these devices have potential applications in local field magnetometry, as is conventionally done with Superconducting Quantum Interference Devices (SQUIDs). These devices can also be used to image super current phase profiles, and could have applications as superconducting phase gradiometers.

Conductive polymers have also been DNA-templated to create nanowire transistors. Hamed et al.⁹⁷ have utilised intrinsically conducting polymers, using λ -DNA as the polymerisation template for conductive poly(3,4-ethylenedioxythiophene), (PDOT)S. This method turns the DNA molecule into a uniform and dynamic semiconductor-conductor hybrid in water, with minimal disruption to the DNA self-assembling properties. The transistor construction and performance are shown in figure 31.

A previous study by Nilsson and Ingnas⁹⁸ has demonstrated that DNA retains its base pair matching capabilities in the presence of fluorescence conjugated polyelectrolytes. This ability, combined with the similarity between conducting polymers and DNA in their organic polymeric nature could lead to further evolution of intrinsically conducting polymeric materials, allowing for massively parallel self-assembly schemes where both polymer conductors and semiconductors can be manipulated to a very high degree of accuracy in 3D.

Conducting DNA-templated nanowires can also be used as ultra-sensitive hydrogen gas sensors. This has been demonstrated by Al-Hinai et al.^{86, 99} In this study, DNA-templated Pd nanowires were produced using aqueous DNA templating reactions. The nanowires were shown to have a granular structure with a very small grain size (<2 nm) and displayed ohmic behaviour. A simple combing technique was used to deposit the DNA-templated nanowires onto a hydrophilic Si/SiO₂ substrate, forming a network of interconnected nanowires. An advantage of using networks is that they allow multiple routes for current to flow. The resistance of these networks increases in a reversible manner upon exposure to H₂ gas, the sensitivity of these devices also rises between 330 – 400 K, as demonstrated in figure 32. The reason for this change is resistance is due to the formation of Pd hydride (PdHx) at or above room temperature. These nanowire networks are less conductive than bulk Pd but have demonstrated sensitivity down to 1700 ppm hydrogen

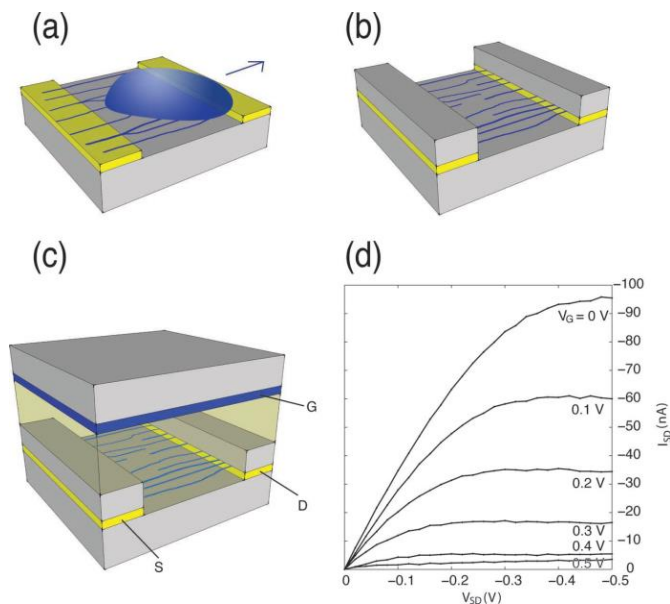


Figure 31: (a) Stretching of λ -DNA/PDOT-S nanowires across microelectrodes. (b) Addition of electrolyte insulation barrier on top of electrodes. (c) PDOT:PSS film acting as a gate (G) with an ionic liquid gel electrolyte in between the channel and the gate. (d) Transistor transfer characteristic I-V curve. From *Small*, Electronic Polymers and DNA Self-Assembled in Nanowire Transistors, **9**, 2013, 363-368, Mahiar Hamed, Anders Elfving, Roger Gabrielsson and Olle Ingnäs. Reprinted with permission from John Wiley and Sons.

with a response rapid times (~85 seconds) as demonstrated in figure 32.

4.2 Fluorescence Resonance Energy Transfer

Fluorescence resonance energy transfer (FRET) is a quantum interaction between two dye molecules. In this process, excitation energy is transferred from a donor to an acceptor fluorophore through dipole-dipole interaction without emitting a photon. The fluorophores typically need to be within 1-10 nm of each other for FRET to occur.¹⁰⁰ The donor molecule becomes quenched and the acceptor molecule becomes excited. The acceptor then dissipates the excited energy through photon emission or thermal energy transfer. When FRET occurs in bulk, donor fluorescence, lifetime and quantum efficiency decrease, leading to an increase in acceptor fluorescence. This change can be easily detected. The theory of FRET was developed by Theodor Förster in the late 1940s¹⁰¹ but FRET-based DNA applications did not emerge until the mid-1980s.¹⁰⁰ Since then, FRET-based techniques using DNA as a scaffold have been further developed, along with a range of applications. One of the biggest advantages of using DNA molecules in this way is that they provide precise control allowing acceptor and donor fluorophores be positioned within 10 nm.

Extensive research has been conducted into the creation of adjacent DNA hybridisation probes, starting in 1988 with a

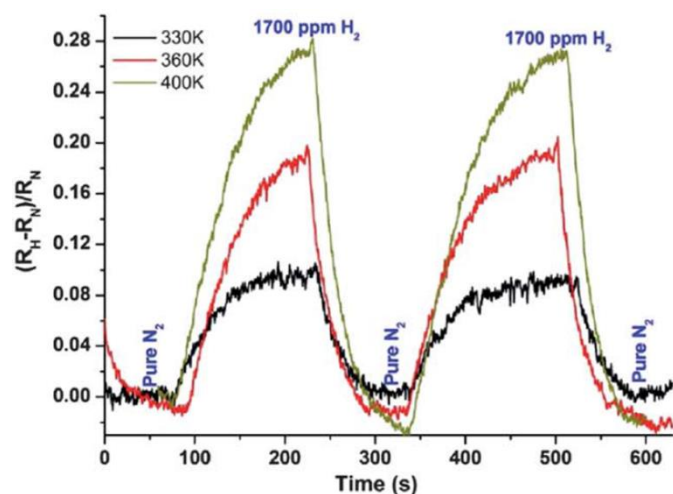


Figure 32: The response of the H₂ sensor upon exposure to 1700 ppm H₂ gas at 330K, 360K and 400K. The sensor demonstrates reversible properties with a response time of ~85 seconds.⁸⁶

study by Cardullo et al.¹⁰² These probes are formed by single strands of DNA with either a donor or acceptor fluorophore on its end. When these come into contact with the right unravelled DNA sequence, they bind to that specific section of the sequence. Donor and acceptor fluorophores can be brought into close proximity if they bind to the right sequence, such as a recognised gene. They would then fluoresce via the acceptors, rather than the donors. These are used to detect genetic diseases for instance. More recently molecular beacons have been developed which operate in the reverse manner to hybridisation probes.¹⁰³ These beacons are formed of a single self-assembled hairpin type structure made out of ssDNA with a donor and acceptor fluorophore held in close proximity at opposite ends as shown in figure 33. The acceptor acts as a quencher for the donor. When they react with the right sequence, they unravel, separating the donor from the acceptor, allowing the donor to fluoresce. This change in fluorescence can be detected and used to identify specific gene sequences. These probes are shown in figure 33.

DNA-templated FRET is applied in PCR technology, i.e. the mass duplication of strands of DNA. It is used to monitor progress of the reaction. The energy transfer probes can be cleaved, as with TaqMan® probes,¹⁰⁴ merged into an amplified DNA, as with scorpion primers¹⁰⁵ or change shape in the presence of a complementary DNA target, as with molecular beacons.¹⁰⁶ In all cases, the probes emit a signal due to the elimination of a quenching influence on the donor fluorophore.

DNA based biosensors can also be made using FRET in a developing field. These systems use complex enzyme probe structures which are far more complicated than previously mentioned FRET applications.¹⁰⁰ An example biosensor uses deoxyribosome based FRET probes to detect Pb ions.¹⁰⁷ The research found a DNA oligonucleotide which cleaves substrate RNA

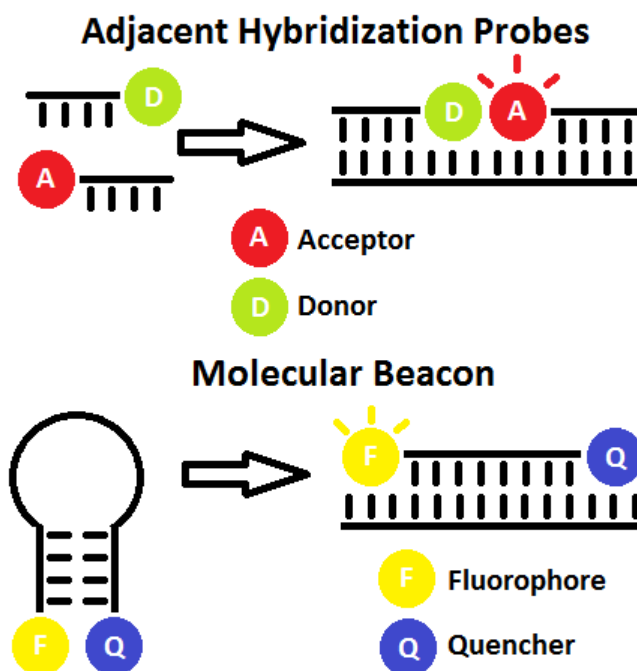


Figure 33: The design of adjacent hybridization probes and molecular beacons. Adjacent probes operate by transferring energy between donor and acceptor fluorophores at close range, prompting emission from the acceptor. Molecular beacons operate by increasing the distance between donor and acceptor fluorophores, enabling the donor to fluoresce, rather than the acceptor.¹⁰⁰

when an ionised lead cofactor is present. In the setup, catalytic DNA is labelled with a fluorescent quencher, i.e. an acceptor molecule and the RNA substrate is labelled with a fluorescent tag, i.e. a donor fluorophore. As with molecular beacon probes mentioned earlier, the fluorescent signal is initially suppressed due to the close proximity of the quenching molecule to the fluorophore. This proximity is broken when the lead cofactor is present, as substrate RNA is cleaved, releasing the fluorescent tag into the solution. This sensor was 80 times more sensitive to Pb than other divalent metal ions, but the approach could be applied to the detection of a wide range of chemical components.

DNA based FRET technology is already well established in the fields of DNA, RNA and protein characterisation and monitoring. In addition to the examples above, it can also be used for DNA mutation detection,¹⁰⁸ DNA cleavage detection,¹⁰⁹ DNA ligation detection,¹¹⁰ DNA recombination detection,¹¹¹ RNA synthesis monitoring¹¹² and energy transfer sequencing monitors.¹¹³ FRET is able to detect and monitor many of the reactions in live cells, making it a valuable tool for in vivo visualisations of cellular processes. FRET sensors also allow real-time monitoring of DNA amplification in PCR. It allows the simultaneous detection of multiple products and is well suited for clinical diagnostics.¹⁰⁰

Early studies by Kawahara et al.^{114, 115} demonstrated the use of an additional chromophore placed between two long range

chromophores (with a separation of 8 nm) that was able to increase the efficiency of FRET by 50%. DNA was used as the backbone template for this study, suggesting that the precise control offered by DNA templating could be used to improve the efficiency of some biosensors. It was also suggested that this method could be used to produce a sequential series of chromophores, capable of providing information on the distance between chromophores separated by more than 10 nm. These extended photonic wires could have a range of applications, including photonic nano circuits and alternative or enhanced biosensors.

4.3 DNA Cetyltrimethylammonium (CTMA)

DNA-CTMA is a DNA scaffolded material produced by adding commercially available hexadecyl trimethyl ammonium chloride to purified DNA. During synthesis, cetyltrimethylammonium (CTMA) binds to the backbone of purified DNA, releasing NaCl as a by-product as shown in figure 34.¹¹⁶ DNA-CTMA has higher structural resilience than conventional DNA due to the long alkyl chains of CTMA and is no longer water soluble due to the hydrophobic nature of CTMA; it does however become chemically soluble in solvents such as chloroform, ethanol, methanol, butanol and chloroform-alcohol blends which are more compatible with device fabrication. DNA-CTMA films can be cast using standard methods, such as spin coating, doctor blading, dip coating and drop casting etc. It is has very high transmission properties over a broad range of wavelengths and is a low-loss optical material with a refractive index ranging from 1.562 to 1.540. DNA-CTMA films with molecular weights of 500,000 and 6,500,000 as a function of temperature have electrical resistivities in the range of $10^9 - 10^{14} \Omega \cdot \text{cm}$. The dielectric constant of DNA CTMA is in the range of 7.8 – 6 for a frequency range of 1 – 1,000 kHz. DNA-CTMA shows thermal stability up to 230 °C via thermo-gravimetric analysis and has 10% water absorption in air at room temperature. These properties make DNA-CTMA an attractive area of research for optical and electronic applications.

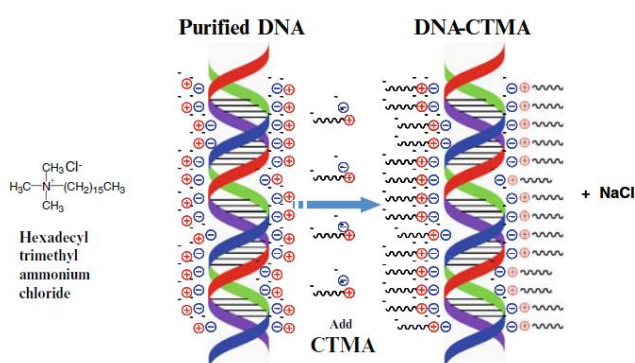


Figure 34: The synthesis process for DNA CTMA. Hexadecyl trimethyl ammonium chloride is combined with purified DNA, easily extracted from fishing industry waste such as salmon milt and roe sacs. The cetyltrimethylammonium then binds to the DNA backbone, releasing NaCl as a by-product. With kind permission from Springer Science+Business Media: *Advances in Polymer Science*, Bio-Organic Optoelectronic Devices Using DNA, **223**, 2010, 189-212, Thokchom Birendra Singh, Niyazi Serdar Sariciftci, and James G. Grote, figure 5.

4.4 Organic Field Effect Transistors (OFETs)

Traditional Organic FETs (OFETs) use semiconducting materials with low electron mobilities and organic oxide materials as a gate with low dielectric constants. As a result the devices are slow and require high operating voltages when compared to inorganic silicon based equivalents. Singh et al have used spin coated DNA-CTMA as the gate dielectric region,¹¹⁷ yielding devices with promising I-V properties compared to traditional OFETs.

Organic dielectrics offer several advantages over their inorganic counterparts.¹¹⁶ They can be solution processed. They provide smooth films on transparent glass and plastic substrates. They are suitable for optoelectronics due to their high optical transparency, making them strong candidates for photo-responsive OFETs. They are also thermally stable up to 200 °C with a small thermal expansion coefficient.

DNA-CTMA is a good material for dielectric layers in OFETs. It is a relatively smooth and forms a better dielectric interface for charge transport from the organic semiconducting material. It also has a large capacitive coupling due to its high dielectric constant of 7.8. Bio OFETs (BioFETs) can be made in a variety of ways, but the study by Singh et al¹¹⁷ focussed on using top contact geometry, evaporating a 50 nm thick pentacene organic semiconductor film onto a 200 nm thick layer of DNA-CTMA, which served as a gate dielectric. The design of this BioFET is shown in figure 35. This transistor was able to modulate drain current over three orders of magnitude using gate voltages of less than 10 V. The transfer characteristics also demonstrate pronounced hysteresis, possibly due to the motion of ionic charges at the semiconductor interface. The linear mobility of the device was measured to be $10^{-2} \text{ cm}^2/\text{V}\cdot\text{s}$. This demonstrates a promising low gate voltage BioFET, potentially rendering OFETs competitive for low frequency applications. These devices are advantageous from a low cost, high volume perspective as the materials are inexpensive and can be spin deposited without any special processing.

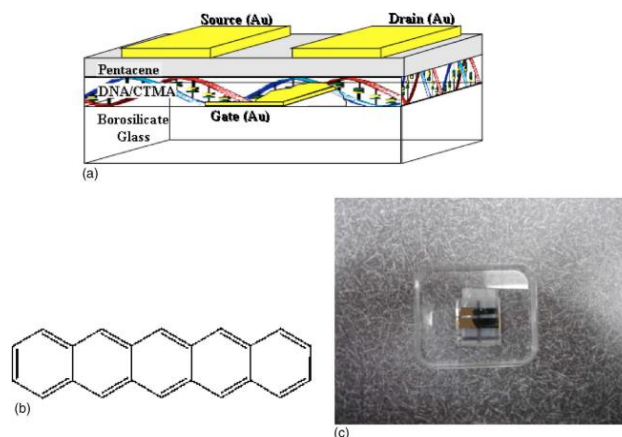


Figure 35: (a) The DNA-CTMA BioFET layout. (b) The chemical structure of pentacene. (c) Photograph of the BioFET device. Reprinted with permission from the *Journal of Applied Physics*, **100**, 2006, 024514, Birendra Singh, Niyazi Serdar Sariciftci, James G. Grote and Frank K. Hopkins. Copyright 2006 AIP Publishing LLC.

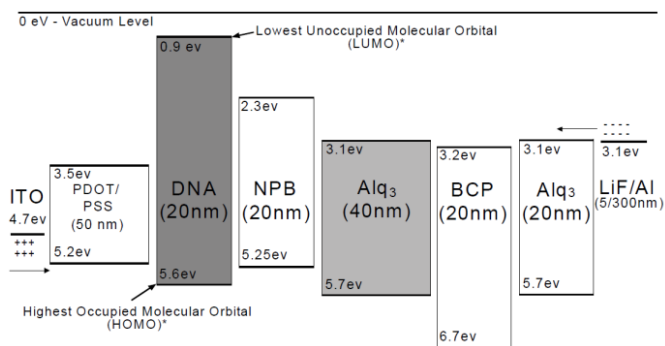


Figure 36: The design specifications of the green Alq3 OLED consisting of a PDOT:PSS hole injection layer, a DNA-CTMA EBL, a NPB hole transport layer, an Alq3 emission layer, a BCP hole blocking layer and a Alq3 electron transport layer. To make the blue OLEDs the Alq3 layer was removed and for the comparative OLEDs either PVK, PMMA or nothing was used in place of the DNA-CTMA EBL. Reprinted with permission from *Applied Physics Letters*, **88**, 2006, 171109, Hagen, J. A. Li, W. Steckl, A. J. and Grote, J. G. Copyright 2006 AIP Publishing LLC.

4.5 Organic Light Emitting Diodes (OLEDs)

A study by Hagen et al.¹¹⁸ has shown that by incorporating DNA-CTMA into fluorescent type Organic Light Emitting Diodes (OLEDs) as an Electron Blocking Layer (EBL), it is possible to improve device efficiency by 2 – 10 times, making them up to 30 times brighter compared to OLEDs with no EBL, a polyvinyl carbazole (PVK) EBL or a polymethylmethacrylate (PMMA) EBL. DNA-CTMA was used on both a green and blue OLED. The green OLED consists of an indium tin oxide (ITO) anode, a 50 nm PDOT:PSS hole injection layer, a 20 nm DNA-CTMA EBL, a 20 nm NPB [(N,N'-bis(naphthalene-1-yl)-N,N'-bis(phenyl)benzidine)] hole transport layer, a 40 nm Alq3 [tris-(8-hydroxyquinoline)

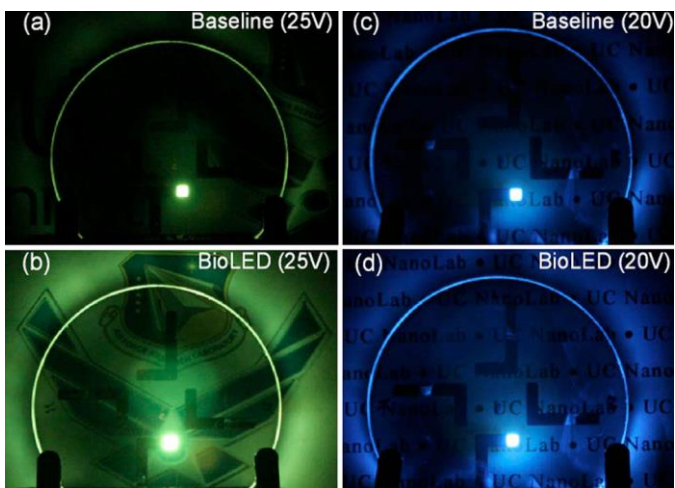


Figure 37: Photographs of (a) Green Alq3 baseline OLED with no EBL at 25 V. (b) Green Alq3 baseline OLED with a DNA-CTMA EBL at 25 V. (c) A blue NPB baseline OLED with no EBL at 20 V. (d) A blue NPB baseline OLED with a DNA-CTMA EBL at 20 V. The emitting areas are 2 mm x 2 mm. Reprinted with permission from *Applied Physics Letters*, **88**, 2006, 171109, Hagen, J. A. Li, W. Steckl, A. J. and Grote, J. G. Copyright 2006 AIP Publishing LLC.

aluminium] emitter layer, a 20 nm BCP [2,9-dimethyl-4,7-diphenyl-1,10-phenanthroline] hole blocking layer, a 20 nm Alq3 electron transport layer, a LiF electron injection layer and an Al cathode. This is shown in figure 36. Blue OLEDs were made by removing the Alq3 emitting layer, forcing the electron hole recombination to occur in the NPB layer. Reference LEDs were also produced to compare results with these including devices with no EBL, the EBL replaced with PVK and the EBL replaced with PMMA. The main reason for the observed increase in device efficiency and luminance is due to the low DNA-CTMA lowest unoccupied molecular orbit (LUMO) level (0.9 eV), which allows for more efficient electron-hole recombination as it restricts electron flow into the anode region. A visual demonstration of these OLEDs is presented in figure 37.

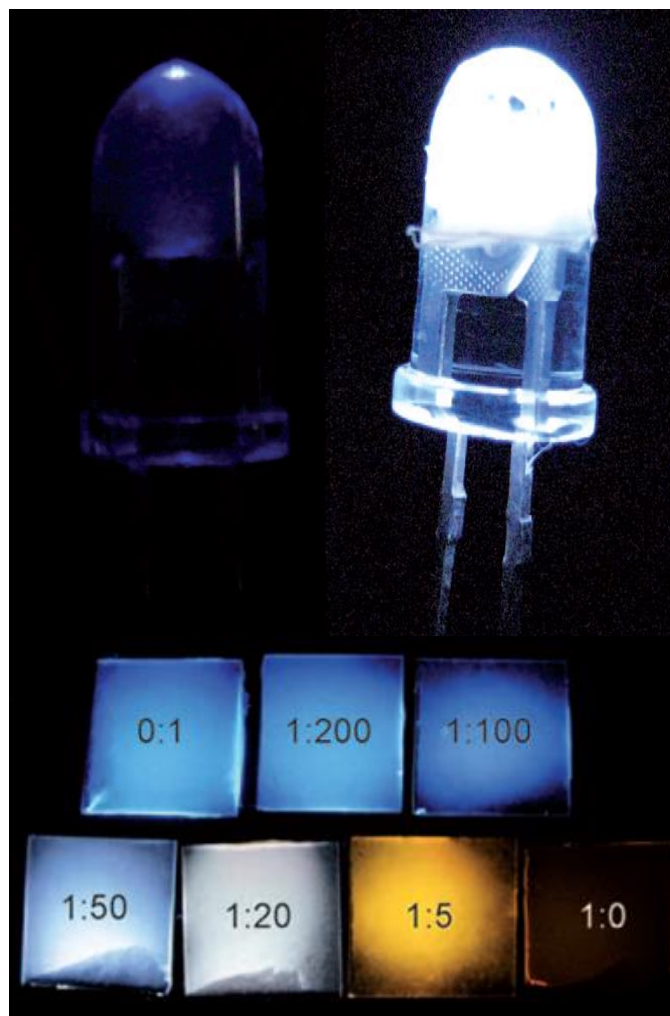


Figure 38: (Top) A UV LED ($\lambda = 400$ nm) without (left) and with (right) a white light emitting nanofibre coating. (Bottom) luminescent nanofibre meshes deposited on glass and illuminated with a UV lamp ($\lambda = 365$ nm). The acceptor to donor ratios are shown. From *Angewandte Chemie International Edition*, White luminescence from multiple-dye-doped electrospun DNA nanofibers by fluorescence resonance energy transfer, **48**, 2009, 5134-5138, Yogesh Ner, James G. Grote, Jeffrey A. Stuart, and Gregory A. Sotzing. Reprinted with permission from John Wiley and Sons.

Ner et al have recently combined the use of DNA-CTMA with FRET in order to create tuneable films for application to LEDs.¹¹⁹ In this study Coumarin 102 (Cm102) and 4-[4-dimethylaminostyryl]-1-docosylpyridinium bromide (Hemi22) were used as donor and acceptor fluorophores. These are able to associate with DNA through different mechanisms. When these are spin deposited into a thin film of DNA-CTMA, the result is a distribution of immobilized dye molecules spaced in a manner which favours efficient energy transfer, even at low acceptor loading levels. The emission wavelength is determined by the ratio of donors to acceptors, which using Cm102 and Hemi22 allows for fluorescence from blue to orange through pure white, as shown in figure 38. DNA facilitates this emission by providing spatial organisation and specific binding environments for the dye molecules. The emission intensity is enhanced by the geometry of the spin deposited fibres.

This technology is exciting as the prospect of all-organic, non-phosphor based white light technology is beneficial in terms of environmental disposal and the utilisation of a renewable resource.

5. Future Outlook

The DNA Biopolymer has two key features that provide the basis for its future implementation. The information encoded in DNA gives instructions for autonomous processes, including the self-assembly of specifically designed nanostructures. These nanostructures can exhibit novel functionalities, including the formation of catalytic nanostructures, the control of electrical properties on surfaces and programmable nanostructures with accurate spatial control of the position of proteins or nanoparticles.¹²⁰ The amazing progress of DNA nanotechnology over the last 30 years is expected to have an impact in a wide variety of disciplines including electronics, photonics, biomedical engineering, biosensing, therapeutics and nucleic-acid-based drug delivery.¹²¹ DNA templated structures provide a platform for mechanical, chemical and physical devices. The next step will be to develop advanced structures that have viable physical, chemical and biological applications. DNA computation is at an early stage of development, but future development of novel ways to use DNA could also lead to a large role in biological computation and data storage.¹²²

6. Conclusions

DNA is far more than simply a method of encoding genetic information. As a convenient and naturally occurring 1D material, it may act as an effective template for the self-assembly of a wide variety of materials with many interesting properties and applications.

The synthesis of DNA-templated 1D structures is a varied and constantly evolving process. Whilst genomic DNA templates are commonly used for nanowire synthesis, the self-assembly approach employed varies markedly between materials. Metallic and semiconductor structures are formed using DNA-bound metallic cations that are either reacted with a reducing agent, or chalcogenide compound respectively. Whilst magnetic nanowires have been

formed using cationic NPs, an electrochemical reduction technique was recently introduced. Lastly, polymeric structures have been produced via the polymerisation of cationic monomers along the polyanionic DNA backbone; with one recent study doing so between adsorbed NPs to bestow unique electronic properties. The methodologies employed in the self-assembly of discrete NP arrays showed similar variability within material groups; including Au NPs functionalised with oligonucleotides; DNA-binding peptides; or streptavidin and bound to synthetic periodic DNA templates. Such synthetic DNA has been used to produce complex supramolecular DNA assemblies for templating. However, DNA origami of genomic DNA provides the means to create complex template geometries onto which NPs can be selectively seeded, and as such is perhaps one of the most exciting advances in recent years.

Thorough characterisation of structures templated on DNA reveals their many and varied interesting properties. Imaging techniques allow quick and easy qualitative analysis, providing morphological and dimensional information. This plays an important role in supporting other, more quantitative methods. The electrical characterisation of nanowires is a major part of the research effort in this field. Metallic nanowires and conducting polymers offer many opportunities for creating nano-scale circuitry and devices with novel electronic properties. A wide range of spectroscopic techniques are used for chemical analysis and monitoring of the self-assembly process. In particular, UV-Vis absorption spectra facilitate the development of optical applications.

The applications of DNA-templated nanotechnology are wide and varied. The examples provided give a feel for different ways that DNA can be applied. Conductive nanowires for use in complex programmable nano circuitry are an area of interest as they potentially allow for the self-assembly of electrical components, which would not be possible with conventional lithography techniques. Several devices have been constructed already using these methods, such as a DNA-templated Carbon Nanotube FETs, quantum interference devices, and gas sensors. A range of metals and conductive materials have been used to develop conducting wires. DNA-templated applications in biosensing have been under extensive research since the 1980s using FRET as the principle detection mechanism. DNA-CTMA has been recognised as a material with impressive potential, examples have been given of its use in creating improved OFETs, more efficient LEDs and tuneable LEDs.

One commonly cited hurdle to the wide-scale realisation of these devices is the cost of DNA synthesis. Although the cost to sequence DNA has outpaced Moore's Law since 2008, DNA synthesis remains relatively expensive. Despite the price falling over the last number of decades, oligonucleotide synthesis is ~US \$0.40 per base, and this value increases to dollars-per-base with constructs kilobases in length.¹²³ Furthermore, nucleotide base errors are increasingly apparent with constructs greater than 200 bases. However, recent technological advances aim to produce longer, more accurate constructs at lower cost.¹²³ Conversely, Zhang et al have suggested that this problem of DNA synthesis scalability is exaggerated,

calculating the material cost of a DNA template to be less than \$6 per m².¹²⁴

Acknowledgements

The authors acknowledge the Engineering and Physical Science Research Council (EPSRC) North West Nanoscience Doctoral Training Centre (NOWNANO DTC) grant reference EP/G017905/1.

Notes and references

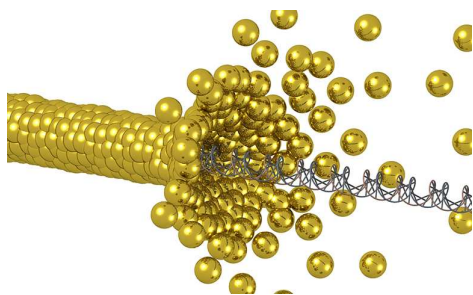
^a North-West Nanoscience Doctoral Training Centre, The University of Manchester, Manchester, Manchester M13 9PL, UK.

^b School of Materials, The University of Manchester, Manchester M13 9PL, UK. E-mail; aravind@manchester.ac.uk

- G. M. Whitesides and B. Grzybowski, *Science*, 2002, **295**, 2418-2421.
- G. M. Whitesides and M. Boncheva, *Proceedings of the National Academy of Sciences of the United States of America*, 2002, **99**, 4769-4774.
- B. Alberts, D. Bray, J. Lewis, M. Raff, K. Roberts and J. D. Watson, *Garland, New York*, 1994.
- G. M. Whitesides, *Sci. Am.*, 1995, **273**, 146-149.
- Z. T. a. N. A. Kotov, *Advanced Materials*, 2005, **17**, 951-962.
- C. M. Lieber, *Solid State Communications*, 1998, **107**, 607-616.
- S. Pruneanu, S. A. F. Al-Said, L. Dong, T. A. Hollis, M. A. Galindo, N. G. Wright, A. Houlton and B. R. Horrocks, *Advanced Functional Materials*, 2008, **18**, 2444-2454.
- K. V. Gothelf and T. H. LaBean, *Organic & biomolecular chemistry*, 2005, **3**, 4023-4037.
- J. Richter, *Physica E*, 2003, **16**, 157-153.
- S. Beyer, P. Nickels and F. C. Simmel, *Nano letters*, 2005, **5**, 719-722.
- R. Hassanien, M. Al-Hinai, S. A. Farha Al-Said, R. Little, L. Siller, N. G. Wright, A. Houlton and B. R. Horrocks, *ACS Nano.*, 2010, **4**, 2149-2159.
- Z. Deng and C. Mao, *Nano letters*, 2003, **3**, 1545-1548.
- A. Ongaro, G. F., P. Beecher, L. Nagle, D. Iacopino, A. Quinn, G. Redmond and D. Fitzmaurice, *Chem. Mater.*, 2004, **17**, 1959-1964.
- S. Kundu and M. Jayachandran, *RSC Advances*, 2013, **3**, 16486.
- A. C. Pearson, J. Liu, E. Pound, B. Uprety, A. T. Woolley, R. C. Davis and J. N. Harb, *The journal of physical chemistry. B*, 2012, **116**, 10551-10560.
- S. H. Park, R. Barish, H. Li, J. H. Reif, G. Finkelstein, H. Yan and T. H. LaBean, *Nano letters*, 2005, **5**, 693 - 696.
- I. Cheng, B. Wei, X. Zhang, Y. Wang and Y. Mi, *Research Letters in Nanotechnology*, 2008, **2008**, 1-4.
- D. Coomber, D. Bartczak, S. R. Gerrard, S. Tyas, A. G. Kanaras and E. Stulz, *Langmuir : the ACS journal of surfaces and colloids*, 2010, **26**, 13760-13762.
- E. Pound, J. R. Ashton, H. A. Becceril and A. T. Woolley, *9*, 2009, **12**, 4302-4305.
- Z. Deng, Y. Tian, S. H. Lee, A. E. Ribbe and C. Mao, *Angewandte Chemie*, 2005, **44**, 3582-3585.
- K. M. M. Carneiro, G. D. Hamblin, K. D. Hänni, J. Fakhoury, M. K. Nayak, G. Rizis, C. K. McLaughlin, H. S. Bazzi and H. F. Sleiman, *Chemical Science*, 2012, **3**, 1980.
- C. Russell, K. Welch, J. Jarvius, Y. Cai, R. Brucas, F. Nikolajeff, P. Svedlindh and M. Nilsson, *ACS Nano*, 2014, **8**, 1147 - 1153.
- P. W. Rothmund, *Nature*, 2006, **440**, 297-302.
- Y. Geng, J. Liu, E. Pound, S. Gyawali, J. N. Harb and A. T. Woolley, *Journal of Materials Chemistry*, 2011, **21**, 12126.
- H. Bui, C. Onodera, C. Kidwell, Y. Tan, E. Graugnard, W. Kuang, J. Lee, W. B. Knowlton, B. Yurke and W. L. Hughes, *Nano letters*, 2010, **10**, 3367-3372.
- Y. Geng, A. C. Pearson, E. P. Gates, B. Uprety, R. C. Davis, J. N. Harb and A. T. Woolley, *Langmuir : the ACS journal of surfaces and colloids*, 2013, **29**, 3482-3490.
- A. Kuzyk, R. Schreiber, Z. Fan, G. Pardatscher, E. M. Roller, A. Hogege, F. C. Simmel, A. O. Govorov and T. Liedl, *Nature*, 2012, **483**, 311-314.
- Q. Gu, C. Cheng, R. Gonela, S. Suryanarayanan, S. Anabathula, K. Dai and D. T. Haynie, *Nanotechnology*, 2006, **17**, R14-R25.
- B. Li, W. Han, M. Byun, L. Zhu, Q. Zou and Z. Lin†, *ACS Nano*, 2013, **7** 4326-4333.
- S. R. M. and A. T. Woolley, *Biomed Microdevices.*, 2004, **6**, 105-111.
- J. Li, C. Bai, C. Wang, C. Zhu, Z. Lin, Q. Li and E. Cao, *Nucleic Acids Res.*, 1998, **26**, 4785-4786.
- S. M. Watson, H. D. Mohamed, B. R. Horrocks and A. Houlton, *Nanoscale*, 2013, **5**, 5349-5359.
- K. Nguyen, M. Monteverde, A. Filoramo, L. Goux-Capes, S. Lyonnais, P. Jegou, P. Viel, M. Goffinan and J.-P. Bourgoïn, *Advanced Materials*, 2008, **20**, 1099-1104.
- J. Liu, B. Uprety, S. Gyawali, A. T. Woolley, N. V. Myung and J. N. Harb, *Langmuir : the ACS journal of surfaces and colloids*, 2013, **29**, 11176-11184.
- W. Monson and A. T. Woolley, *Nano letters*, 2003, **3**, 359-363.
- E. Braun, Y. Eichen, U. Sivan and G. Ben-Yoseph, *Nature*, 1998, **391**, 775-778.
- J. Kinsella, M. and A. Ivanisevic, *Int. J. Nanomedicine*, 2006, **1**, 219-222.
- J. Richter, M. Mertig, W. Pompe, I. Mönch and H. K. Schackert, *Applied Physics Letters*, 2001, **78**, 536.
- H. Yokota, J. Sunwoo, M. Sarikaya, G. van den Engh and R. Aebbersold, *Anal Chem.* , 1999, **71**, 4418-4422.
- B. Teshome, S. Facsko and A. Keller, *Nanoscale*, 2014, **6**, 1790-1796.
- W. U. Dittmer and F. C. Simmel, *Applied Physics Letters*, 2004, **85**, 633.
- J. Richter, R. Seidel, R. Kirsch, M. Mertig, W. Pompe, J. Plaschke and H. K. Schackert, *Adv. Mater.*, 2000, **12**, 507-510.
- Liu, J., Y. Geng, E. Pound, S. Gyawali, J. R. Ashton, J. Hickey, A. T. Woolley and J. N. Harb, *ACS Nano.*, 2011, **5**, 2240-2247.
- K. Keren, R. S. Berman, E. Buchstab, U. Sivan and E. Braun, *Science*, 2003, **302**, 1380-1382.
- R. Schreiber, S. Kempter, S. Holler, V. Schuller, D. Schiffels, S. S. Simmel, P. C. Nickels and T. Liedl, *Small*, 2011, **7**, 1795-1799.

46. S. M. Watson, N. G. Wright, B. R. Horrocks and A. Houlton, *Langmuir : the ACS journal of surfaces and colloids*, 2010, **26**, 2068-2075.
47. H. Kudo and M. Fujihira, *Nanotechnology, IEEE Transactions*, 2006, **5**, 90-92
48. R. Hassanien, S. A. Al-Said, L. Siller, R. Little, N. G. Wright, A. Houlton and B. R. Horrocks, *Nanotechnology*, 2012, **23**, 075601.
49. D. Nyamjav and A. Ivanisevic, *Biomaterials*, 2005, **26**, 2749-2757.
50. J. Kinsella, M. and A. Ivanisevic, *J. Am. Chem. Soc.*, 2005, **127**, 3276-3277.
51. Q. Gu and D. T. Haynie, *Materials Letters*, 2008, **62**, 3047-3050.
52. H. D. Mohamed, S. M. Watson, B. R. Horrocks and A. Houlton, *Nanoscale*, 2012, **4**, 5936-5945.
53. M. G. Warner and J. E. Hutchison, *Nature materials*, 2003, **2**, 272-277.
54. S. M. Watson, J. H. Hedley, M. A. Galindo, S. A. Al-Said, N. G. Wright, B. A. Connolly, B. R. Horrocks and A. Houlton, *Chemistry*, 2012, **18**, 12008-12019.
55. L. Dong, T. Hollis, S. Fishwick, B. A. Connolly, N. G. Wright, B. R. Horrocks and A. Houlton, *Chemistry*, 2007, **13**, 822-828.
56. Y. Ma, J. Zhang, G. Zhang and H. He, *J Am Chem Soc.*, 2004, **126**, 7097-7101.
57. R. Nagarajan, S. Roy, J. Kumar, S. Tripathy, T. Dolukhanyan, C. Sung, F. Bruno and L. Samuelson, *Journal of Macromolecular Science, Part A*, 2001, **38**, 1519-1537.
58. H. K. Moon, H. J. Kim, N.-H. Kim and Y. Roh, *Journal of Nanoscience and Nanotechnology*, 2010, **10**, 3180-3184.
59. P. Nickels, W. U. Dittmer, S. Beyer, J. P. Kotthaus and F. C. Simmel, *Nanotechnology*, 2004, **15**, 1524-1529.
60. G. Wang, H. Tanaka, L. Hong, Y. Matsuo, K. Niikura, M. Abe, K. Matsumoto, T. Ogawa and K. Ijro, *Journal of Materials Chemistry*, 2012, **22**, 13691.
61. J. L. Coffer, S. R. Bigham, R. F. Pinizzotto and H. Yang, *Nanotechnology*, 1992, **3**, 69-79.
62. J. L. Coffer, S. R. Bigham, X. Li, R. F. Pinizzotto, Y. G. Rho, R. M. Pirtle and I. L. Pirtle, *Applied Physics Letters*, 1996, **69**, 3851.
63. L. Dong, T. Hollis, B. A. Connolly, N. G. Wright, B. R. Horrocks and A. Houlton, *Advanced Materials*, 2007, **19**, 1748-1751.
64. S. Kundu, H. Lee and H. Liang, *Inorg Chem.*, 2009, **48**, 121-127.
65. T. Torimoto, M. Yamashita, S. Kuwabata, T. Sakata, H. Mori and H. Yoneyama, *J. Phys. Chem. B.*, 1999, **103**, 8799-8803.
66. M. Artemyev, D. Kisiel, S. Abmiotko, M. N. Antipina, G. B. Khomutov, V. V. Kislov and A. A. Rakhnyanskaya, *J Am Chem Soc.*, 2004, **126**, 10594-10597.
67. V. Stsiapura, A. Sukhanova, A. Baranov, M. Artemyev, O. Kulakovich, V. Oleinikov, M. Pluot, J. H. M. Cohen and I. Nabiev, *Nanotechnology*, 2006, **17**, 581-587.
68. H. A. Becerril, P. Ludtke, B. M. Willardson and A. T. Woolley, *Langmuir : the ACS journal of surfaces and colloids*, 2006, **22**, 10140-10144.
69. T. Nishinaka, A. Takano, Y. Doi, M. Hashimoto, A. Nakamura, Y. Matsushita, J. Kumaki and E. Yashima, *J Am Chem Soc.*, 2005, **127**, 8120-8125.
70. Y. Ruff, T. Moyer, C. J. Newcomb, B. Demeler and S. I. Stupp, *Journal of the American Chemical Society*, 2013, **135**, 6211-6219.
71. F. S. a. A. R. Goulson, *J. Mol. Biol.*, 1975, **94**, 441-448.
72. M. Ronaghi, M. Uhlén and P. Nyrén, *Science*, 1998, **281**, 363-365.
73. K. V. Voelkerding, S. A. Dames and J. D. Durtschi, *Clinical chemistry*, 2009, **55**, 641-658.
74. J. H. Shuo Huang, Shuai Chang, Peiming Zhang, Feng Liang, Shengqin Li, Michael Tuchband, and R. R. a. S. L. Alexander Fuhrmann, *Nat. Nano.*, 2010, **5**, 868-873.
75. J. Zheng, J. J. Birkoft, Y. Chen, T. Wang, R. Sha, P. E. Constantinou, S. L. Ginell, C. Mao and N. C. Seeman, *Nature*, 2009, **461**, 74-77.
76. R. Jungmann, M. Scheible and F. C. Simmel, *Wiley interdisciplinary reviews. Nanomedicine and nanobiotechnology*, 2012, **4**, 66-81.
77. Z. D. a. C. Mao, *Nano letters*, 2011, **3**, 1545-1548.
78. W. Su, V. Bonnard and G. A. Burley, *Chemistry*, 2011, **17**, 7982-7991.
79. R. Jungmann, C. Steinhauer, M. Scheible, A. Kuzyk, P. Tinnefeld and F. C. Simmel, *Nano letters*, 2010, **10**, 4756-4761.
80. A. Houlton, A. R. Pike, M. Angel Galindo and B. R. Horrocks, *Chemical communications*, 2009, 1797-1806.
81. G. Wang, H. Tanaka, L. Hong, Y. Matsuo, K. Niikura, M. Abe, K. Matsumoto, T. Ogawa and K. Ijro, *Journal of Materials Chemistry*, 2012, **22**, 13691.
82. A. Houlton and S. M. D. Watson, *Annual Reports Section "A" (Inorganic Chemistry)*, 2011, **107**, 21.
83. H. Yan, S. H. Park, G. Finkelstein, J. H. Reif and T. H. LaBean, *Science*, 2003, **301**, 1882-1884.
84. D. N. Stephanie Vial, Kevin G. Yager, Alexei V. Tkachenko, and Oleg Gang, *ACS Nano*, 2013, **7**, 5437-5445.
85. S. M. Watson, A. R. Pike, J. Pate, A. Houlton and B. R. Horrocks, *Nanoscale*, 2014, **6**, 4027-4037.
86. M. N. Al-Hinai, R. Hassanien, N. G. Wright, A. B. Horsfall, A. Houlton and B. R. Horrocks, *Faraday Discussions*, 2013, **164**, 71.
87. J. Su and F. Gao, *Materials Letters*, 2013, **108**, 58-61.
88. W. Chen, G. z. Güler, E. Kuruvilla, G. B. Schuster, H.-C. Chiu and E. Riedo, *Macromolecules*, 2010, **43**, 4032-4040.
89. S. Sezi and H. A. Wagenknecht, *Chemical communications*, 2013, **49**, 9257-9259.
90. V. A. Galievsky, V. L. Malinovskii, A. S. Stasheuski, F. Samain, K. A. Zachariasse, R. Haner and V. S. Chirvony, *Photochemical & photobiological sciences : Official journal of the European Photochemistry Association and the European Society for Photobiology*, 2009, **8**, 1448-1454.
91. C. Dekker and M. A. Ratner, *Physics World*, 2001.
92. F. Patolsky, Y. Weizmann, O. Lioubashevski and I. Willner, *Angew. Chem. Int. Ed.*, 2002, **41**, 2323-2327.
93. J. Richter, M. Mertig, W. Pompe, I. Monch and H. K. Schackert, *Appl. Phys. Lett.*, 2001, **78**, 536 - 538.
94. M. Mertig, L. C. Ciacchi, R. Seidel, W. Pompe and A. D. Vita, *Nano Lett.*, 2002, **2**, 841-844.
95. C. F. Monson and A. T. Woolley, *Nano Lett.* 2003, **3**, 359-363, 2003, **3**, 359 - 363.
96. D. S. Hopkins, D. Pekker, P. M. Goldbart and A. Bezryadin, *Science*, 2005, **308**, 1762-1765.
97. M. Hamedi, A. Elfving, R. Gabrielsson and O. Inganas, *Small*, 2013, **9**, 363-368.
98. K. P. Nilsson and O. Inganas, *Nature materials*, 2003, **2**, 419-424.

99. M. Al-Hinai, N. Wright, A. Horsfall, R. Hassanien, B. Horrocks and A. Houlton, *Sensors IEEE*, 2011.
100. V. V. Didenko, *Biotechniques*, 2001, **31**, 1106–1121.
101. T. Förster, *Ann Phys (Leipzig)*, 1948, **2**, 55 - 75.
102. R. A. CARDULLO, S. AGRAWAL, C. FLORES, P. C. ZAMECNIK and D. E. WOLF, *Proc. Natl. Acad. Sci. USA*, 1988, **85**, 8790 - 8794.
103. S. Tyagi and F. R. Kramer, *Nat Biotechnol*, 1996, **14**, 303 - 308.
104. K. J. Livak, S. J. Flood, J. Marmaro, W. Giusti and K. Deetz, *Genome Res.*, 1995, **4**, 357 - 362.
105. N. Thelwell, S. Millington, A. Solinas, J. Booth and B. T., *Nucleic Acids Res* 2000, **28**, 3752 - 3761.
106. E. Ortiz, G. Estrada and P. M. Lizardi, *Mol Cell Probes*, 1998, **12**, 219 - 226.
107. J. Li and Y. Lu, *Journal of the American Chemical Society*, 2000, **122**, 10466 - 10467.
108. C. A. Mein, B. J. Barratt, D. M. G., T. Siegmund, A. N. Smith, L. Esposito, S. Nutland and e. al., *Genome Res* 2000, **10**, 330 - 343.
109. S. S. Ghosh, P. S. Eis, K. Blumeyer, K. Fearon and D. P. Millar, *Nucleic Acids Res* 1994;22:3155–3159, 1994, **22**, 3155 - 3159.
110. V. V. Didenko and P. J. Hornsby, *J Cell Biol*, 1996, **135**, 1369 – 1376.
111. R. Bazemore, M. Takahashi and C. M. Radding, *J Biol Chem* 1997, 1997, **272**, 14672 - 14682.
112. Y. Sei-Iida, H. Koshimoto, S. Kondo and A. Tsuji, *Nucleic Acids Res* 2000;28:E59, 2000, **28**, E59.
113. L. M. Smith, J. Z. Sanders, R. J. Kaiser, P. Hughes, C. Dodd, C. R. Connell, C. Heiner, S. B. H. Kent and e. al., *Nature*, 1986, **321**, 674 - 679.
114. S.-i. Kawahara, T. Uchimaru and S. Murata, *Chem. Commun.*, 1999, 563 - 564.
115. S.-I. Kawahara, T. Uchimaru and S. Murata, *Nucleic Acids Symposium Series*, 1999, **42**, 241 - 241.
116. T. B. Singh, N. S. Sariciftci and J. G. Grote, *Advances in Polymer Science*, 2010, **223**, 189 - 212.
117. B. Singh, N. S. Sariciftci, J. G. Grote and F. K. Hopkins, *Journal of Applied Physics*, 2006, **100**, 024514.
118. J. A. Hagen, W. Li, A. J. Steckl and J. G. Grote, *Applied Physics Letters*, 2006, **88**, 171109.
119. Y. Ner, J. G. Grote, J. A. Stuart and G. A. Sotzing, *Angewandte Chemie*, 2009, **48**, 5134-5138.
120. F. Wang, B. Willner and I. Willner, *Current opinion in biotechnology*, 2013, **24**, 562-574.
121. A. Rangnekar and T. H. Labean, *Accounts of chemical research*, 2014.
122. M. Zahid, B. Kim, R. Hussain, R. Amin and S. H. Park, *Nanoscale Research Letters* 2013, , **8**.
123. M. Goldberg, *Industrial Biotechnology*, 2013, **9**, 10-12.
124. G. Zhang, S. P. Surwade, F. Zhou and H. Liu, *Chemical Society Reviews*, 2013, **42**, 2488-2496.



Metallization of double stranded DNA for templated nanowire formation